## ORIGINAL RESEARCH

A Single *RET* Mutation in Hirschsprung Disease Induces Intestinal Aganglionosis Via a Dominant-Negative Mechanism

Mukhamad Sunardi, Keisuke Ito, Yuya Sato, Toshihiro Uesaka, Mitsuhiro Iwasaki, and Hideki Enomoto

Division of Neural Differentiation and Regeneration, Department of Physiology and Cell Biology, Kobe University Graduate School of Medicine, Hyogo, Japan
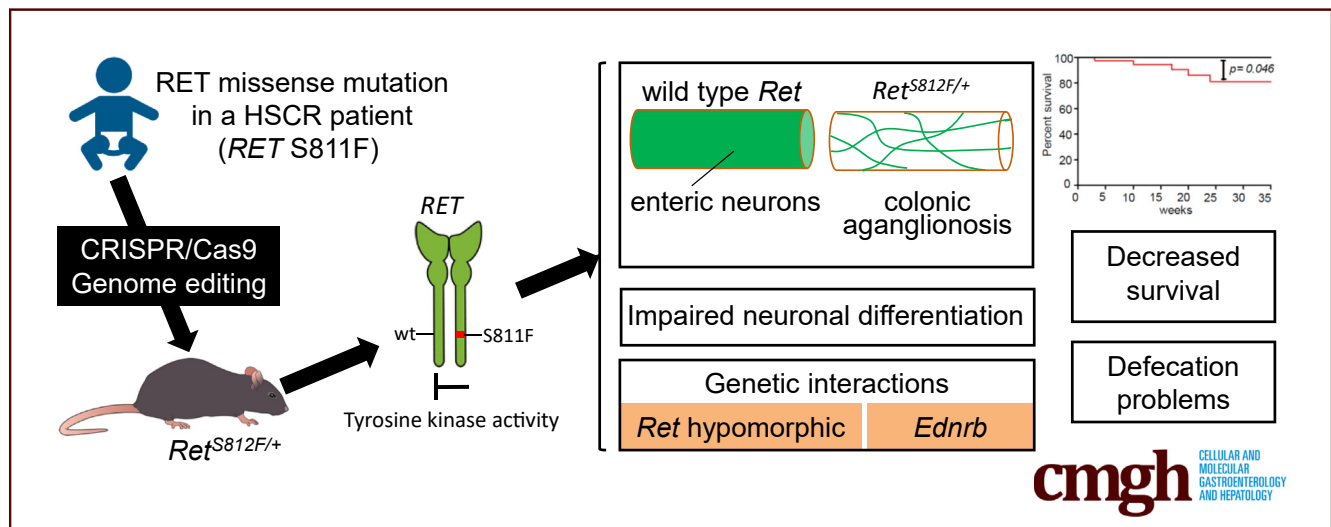
SUMMARY

Introducing a single missense mutation of the *RET* gene identified in Hirschsprung disease recapitulates the disease in mice. The mice further show genetic interactions with other susceptibility gene mutations to exacerbate the disease phenotypes.

BACKGROUND & AIMS: Hirschsprung disease (HSCR) is a congenital disorder characterized by the absence of the enteric nervous system (ENS). HSCR potentially involves multiple gene aberrations and displays complex patterns of inheritance. Mutations of the *RET* gene, encoding the RET receptor tyrosine kinase, play a central role in the pathogenesis of HSCR. Although a wide variety of coding *RET* mutations have been identified, their pathogenetic significance in vivo has remained largely unclear.

METHODS: We introduced a HSCR-associated *RET* missense mutation, *RET*(S811F), into the corresponding region (S812) of the mouse *Ret* gene. Pathogenetic impact of *Ret*(S812F) was assessed by histologic and functional analyses of the ENS and by biochemical analyses. Interactions of the *Ret*(S812F) allele with HSCR susceptibility genes, the *RET9* allele and the *Ednrb* gene, were examined by genetic crossing in mice.

RESULTS: $Ret^{S812F/+}$ mice displayed intestinal aganglionosis (incidence, 50%) or hypoganglionosis (50%), impaired

differentiation of enteric neurons, defecation deficits, and increased lethality. Biochemical analyses revealed that Ret(S811F) protein was not only kinase-deficient but also abrogated function of wild-type RET in trans. Moreover, the *Ret(S812F)* allele interacted with other HSCR susceptibility genes and caused intestinal aganglionosis with full penetrance.

CONCLUSIONS: This study demonstrates that a single *RET* missense mutation alone induces intestinal aganglionosis via a dominant-negative mechanism. The $Ret^{S812F/+}$ mice model HSCR displays dominant inheritance with incomplete penetrance and serves as a valuable platform for better understanding of the pathogenetic mechanism of HSCR caused by coding *RET* mutations. *(Cell Mol Gastroenterol Hepatol 2023; 15:1505–1524; https://doi.org/10.1016/j.jcmgh.2022.12.003)*

Keywords: RET; Hirschsprung Disease; Genetic Interactions; Missense Mutation.

Hirschsprung disease (HSCR) is one of the most frequent gut obstructive conditions in neonates and is caused by the absence of the enteric nervous system (ENS) in the distal gut (intestinal aganglionosis). Genetic studies have identified mutations in more than 30 genes,[1]

among which the *RET* gene is most frequently mutated. The *RET* gene encodes the RET receptor tyrosine kinase that functions as the signaling receptor of the glial cell line-derived neurotrophic factor (GDNF) family ligands after they bind to the glial cell line-derived neurotrophic factor family receptor α (GFRα) receptors.[2] The physiological function of RET in ENS development has been demonstrated by gene targeting studies that showed that homozygous deletion of the *Ret* gene causes nearly complete intestinal aganglionosis below the stomach in mice.[3] *Ret*-deficient mice also display bilateral kidney agenesis. However, *RET* mutations in HSCR are diverse and complex.[4] Non-coding mutations in the *RET* gene are most frequently found and specifically affect the enhancer regions. In isolated HSCR, non-coding *RET* mutations are considered necessary to confer disease susceptibility. However, they alone are not sufficient, and additional gene mutations are required to develop HSCR. Coding *RET* mutations are identified in 50% of familial and 15% of sporadic cases of HSCR. As compared with non-coding mutations, coding mutations are much more diverse and include a variety of deletion, nonsense, and missense mutations. They can occur in any exon in the *RET* gene; there is no known "hot spot" for HSCR-associated coding *RET* mutations. With these genetic features, HSCR families display complex patterns of inheritance.

Although nearly 25 years have passed since coding *RET* mutations in HSCR were first reported,[5,6] their biological significance remains obscure. Previous in vitro studies demonstrated that some of coding *RET* mutations impair RET function, which led to the notion that HSCR-associated mutations are null mutations.[7,8] Because only a few of those mutations have been identified in a homozygous manner, it is generally thought that HSCR is caused by inactivation of 1 copy of the *RET* gene.[9] However, mice lacking 1 copy of the *Ret* gene (*Ret*$^{+/-}$ mice) display nearly normal ENS anatomy. This apparent discrepancy is currently thought to be due to a potential difference in the threshold levels of RET function required for ENS development between these 2 species; halved RET function is sufficient for ENS development in mice but not in humans.[10]

To understand the pathogenetic effect of HSCR-associated coding *RET* mutations, we recently introduced 2 HSCR-associated *RET* missense mutations, *RET*(N394K) and *RET*(Y791F), into the corresponding regions of the mouse *Ret* gene (*Ret*^{N396K} and *Ret*^{Y792F}).[11] Previous studies suggested that *RET*(N394K) and *RET*(Y791F) impair N-linked glycosylation and proper activation of RET, respectively.[12,13] Surprisingly, however, *Ret*$^{N396K/-}$ and *Ret*$^{Y792F/-}$ mice displayed no deficit in the ENS. The fact that single allele expression of only the mutant allele was sufficient for normal ENS development indicated that these RET mutants can exert near normal physiological function in vivo. These results demonstrate that HSCR-associated *RET* mutations are functionally diverse and can even include non-pathogenetic mutations. This also raises a fundamental question: How toxic can a single *RET* missense mutation be in HSCR pathogenesis? Importantly, even to date, it has not been shown whether any of the coding *RET* mutations alone can induce intestinal aganglionosis in vivo. It has also been unclear whether such pathogenetic missense mutations, if any, interact with other gene mutations for the expressivity and severity of HSCR.

To address these issues, we chose a *RET* missense mutation, *RET*(S811F), identified in a HSCR patient associated with unilateral kidney agenesis and oligomeganephronia, a condition characterized by a decrease in nephron numbers. In silico analysis of this mutation suggested that it abrogates RET kinase activity, but no biological evidence was available. We introduced this mutation into the corresponding region (S812) of the mouse *Ret* gene by genome editing. We found that all the *Ret*$^{S812F/+}$ mice showed ENS deficits, either intestinal aganglionosis (50%) or hypoganglionosis (50%). Unilateral kidney agenesis was also found in 10% of the *Ret*$^{S812F/+}$ mice, and their remaining kidneys were smaller in size with decreased numbers of glomeruli. Thus, *Ret*$^{S812F/+}$ mice recapitulated the clinical manifestations of the patient. Biochemical analysis indicated that RET(S811F) exerts dominant-negative effects on wild-type (wt) RET. Furthermore, the *Ret*(S812F) allele exhibited genetic interactions with the *Ret* hypomorphic allele and the endothelin receptor type B (*Ednrb*) gene, and these compound mutations displayed complete penetrance in the intestinal aganglionosis phenotype. *RET*(S811F) represents the most severe form among pathogenetic RET missense mutations, and the *Ret*$^{S812F/+}$ mice provide a valuable platform to understand the pathology, genetic interactions, and pathogenetic mechanisms of HSCR.

Results

HSCR-Associated Missense Mutation, Ret(S812F), Impairs Development of the Enteric Nervous System and Kidney in a Dominant-Negative Fashion

To assess the pathogenetic potential of coding *RET* mutations, we chose to examine a missense mutation, *RET*(S811F), identified in a heterozygous fashion in a HSCR patient. The patient also displayed unilateral kidney agenesis and oligomeganephronia.[14] *RET*(S811F) is localized at the kinase domain of the RET protein (Figure 1*A*), and in silico analysis using AlphaFold Protein Structure Database (https://alphafold.ebi.ac.uk/) shows that this mutation Serine 811 is located at the opening of the adenosine triphosphate binding pocket. Conversion of Serine 811 to
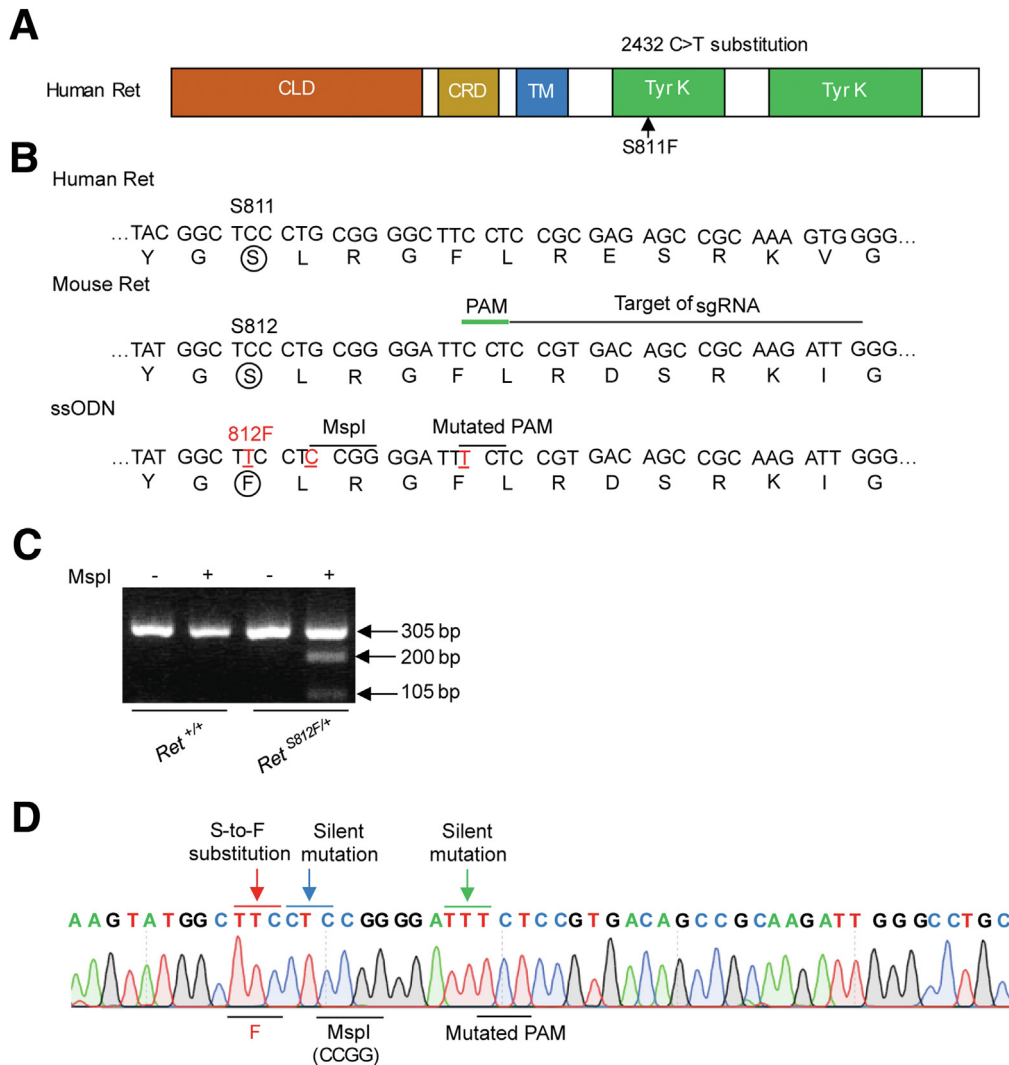
Most current article

Figure 1. Generation of mice harboring the *Ret*(S812F) missense mutation. (A) Schematic shows location of the *Ret*(S811F) mutation in human RET protein. CLD, cadherin-like domain; CRD, cystein-rich domain; TM, transmembrane domain; Tyr K, tyrosine kinase domain. (B) Strategy for introducing the *Ret*(S812F) mutation into the mouse *Ret* gene. Sequence of the human *RET* (*top*) and mouse *Ret* (*middle*) harboring the missense mutation and designed single-stranded oligo DNA nucleotides (*bottom*) are shown. Altered amino acids (S to F) by the mutation are *encircled*. Overline (*green*); PAM (NGG) and the following sequences targeted by the sgRNA. Two silent mutations, one disrupting PAM (TTC>TTT) and the other generating a new MspI site shown in *red letters*. (C) Representative genotyping results of wild-type and heterozygous mutant. After MspI digestion of PCR products, wild-type vs mutant bands appear as 305 bp vs 200 bp and 105 bp, respectively. (D) Sequence chromatogram of the *Ret*(S812F) allele showing *Ret*(S812F) missense mutation (*red*), MspI site (*blue*), and mutated PAM (*green*).

phenylalanine is likely to inhibit adenosine triphosphate binding in the kinase pocket because a bulky side chain of Phenylalanine 811 will block the opening of the pocket.[14] We introduced the *RET*(S811F) mutation into the corresponding site of the mouse *Ret* gene (S812F) by electroporation-mediated genome editing in mouse embryos. In brief, mouse zygotes (3 hours after in vitro fertilization) were subjected to electroporation in medium containing gRNA, Cas9, and single-stranded oligo DNA nucleotides. The single-stranded oligo DNA nucleotides harbored the S812F mutation and 2 silent mutations, one of which disrupted the protospacer adjacent motif sequence and the other introduced the MspI site for genotyping (Figure 1*B*).

Mice were screened by polymerase chain reaction (PCR) and successive MspI digestion of the PCR product (Figure 1*C*). Sequencing analysis on the genomic DNA of mice displaying the expected restriction digestion pattern revealed successful insertion of the desired mutations (Figure 1*D*).

To evaluate the function of the *Ret(S812F)* allele in vivo, we crossed *Ret*^S812F/+ mice with *Ret*^+/tauLacZ mice. The *Ret-tauLacZ* allele is the *Ret*-null allele expressing *tauLacZ* cDNA under the *Ret* promoter, which enables the detection of *Ret*-expressing cells by X-gal staining.[15,16] *Ret*^S812F/tauLacZ embryos (embryonic day 12.5, E12.5) displayed absence of developing ENS below the stomach and absent kidneys (Figure 2*A*, white arrowheads and white arrows,
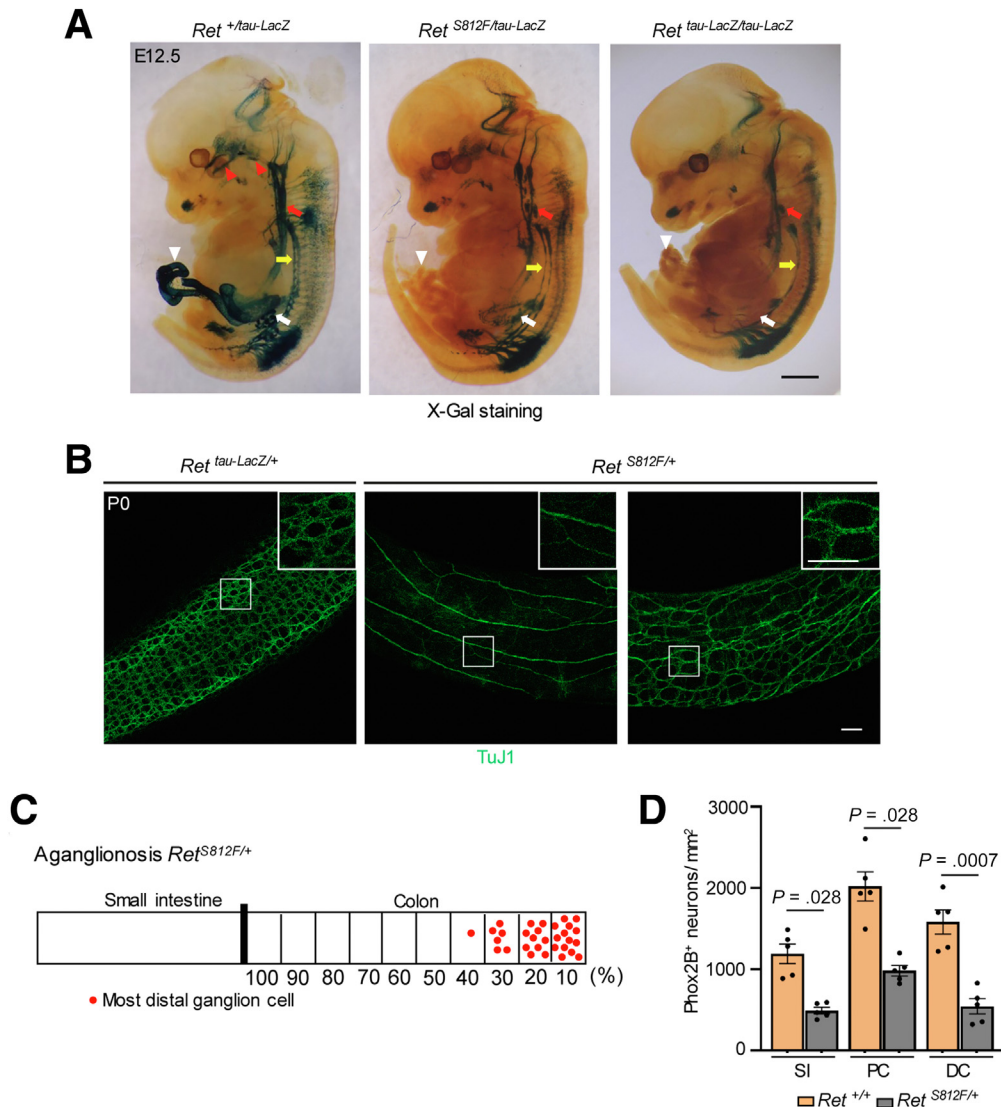
Figure 2. Ret(S812F) impairs ENS development. (*A*) Representative images of whole-mount X-gal staining of $Ret^{+/tau-LacZ}$, $Ret^{S812F/tau-LacZ}$, and $Ret^{tau-LacZ/tau-LacZ}$ mouse embryos (E12.5). Small bowel (*white arrowhead*) and kidney (*white arrow*) are missing in $Ret^{S812F/tau-LacZ}$ and $Ret^{tau-LacZ/tau-LacZ}$ animals (n = 3 per group). *Red arrowheads*; cranial parasympathetic ganglia, *red arrows*; SCG, *yellow arrows*; sympathetic chain. (*B*) Whole-mount TuJ1 immunostaining of colon of newborn $Ret^{tau-LacZ/+}$ and $Ret^{S812F/+}$ mice. Dense meshwork by enteric ganglia in $Ret^{tau-LacZ/+}$ mice (*left*). In $Ret^{S812F/+}$ mice, enteric ganglia are either completely missing (intestinal aganglionosis, *middle*) or much sparser (hypoganglionosis, *right*) than in $Ret^{tau-LacZ/+}$ mice. (*C*) Position of the most distal ganglion cell in mice with distal colon aganglionosis (*red dot*) (n = 31). (*D*) Graph shows density of Phox2B+ neurons in hypoganglionic bowel of $Ret^{S812F/+}$ mice (n = 5 per group). Unpaired two-tailed *t* test with Welch's correction. DC, distal colon; PC, proximal colon; SI, small intestine. Scale bars: (*A*) 0.1 cm, (*B*) 100 μm.

respectively). They also lacked cranial parasympathetic ganglia (Figure 2*A*, red arrowheads) and showed thin sympathetic chains (Figure 2*A*, yellow arrows) with impaired rostral migration of the superior cervical ganglia (Figure 2*A*, red arrows). The phenotype of $Ret^{S812F/tauLacZ}$ embryos resembled that of $Ret^{tauLacZ/tauLacZ}$ (*Ret*-deficient) embryos (Figure 2*A*). These data suggest that the *Ret(S812F)* allele exerts no physiological function in vivo

(*Ret*-null) at least at this developmental period. We next examined the phenotype of the ENS of $Ret^{S812F/+}$ mice because these mice recapitulate the patient's genetic condition (heterozygous mutation). We found that all $Ret^{S812F/+}$ newborn mice displayed deficits in the ENS. Half of them exhibited intestinal aganglionosis with varying lengths of aganglionic regions in the colon (Figure 2*B*, middle, and *C*), and the other half exhibited hypoganglionosis (Figure 2*B*,

Table 1. Incidence of Intestinal Aganglionosis and Kidney Agenesis in Newborn $Ret^{S812F/+}$, $Ret^{S812F/RET9}$, and $Ret^{S812F/+}$; $Ednrb^{+/-}$

	Phenotype	$Ret^{S812F/+}$			$Ret^{S812F/RET9}$			$Ret^{S812F/+}$; $Ednrb^{+/-}$		
		Male	Female	Total (ratio)	Male	Female	Total (ratio)	Male	Female	Total (ratio)
ENS	Normal	0	0	0 (0%)	0	0	0 (0%)	0	0	0 (0%)
	Oligo-ganglionosis	17	14	31 (50.0%)	0	0	0 (0%)	0	0	0 (0%)
	Aganglionosis	13	18	31 (50.0%)	9	12	21 (100%)	10	2	12 (100%)
Fisher exact *P* value			.44			1			1	
Kidney	Two kidneys	27	28	55 (88.7%)	7	11	18 (85.7%)	9	2	11 (91.6%)
	Unilateral kidney agenesis	3	4	7 (11.3%)	1	0	1 (4.8%)	1	0	1 (8.4%)
	Bilateral kidney agenesis	0	0	0 (0%)	1	1	2 (9.5%)	0	0	0 (0%)

NOTE. *P* values (Fisher exact test) for the difference in the incidence of intestinal aganglionosis between male and female animals.

right, and *D*; Table 1). There was no difference in the incidence of intestinal aganglionosis between male and female animals (Table 1, Figure 12*B*). Furthermore, we found that approximately 10% of $Ret^{S812F/+}$ mice displayed unilateral kidney agenesis (Table 1, Figure 8*A*). There was also a reduction in glomeruli numbers in the remaining kidney of $Ret^{S812F/+}$ mice displaying unilateral kidney agenesis (Figure 8*B* and *C*). The phenotype of $Ret^{S812F/+}$ mice contrasted that of the $Ret^{+/tauLacZ}$ mice (equivalent to $Ret^{+/-}$ mice), which display normal development of the ENS and kidneys.[17] These data collectively suggest that the *Ret*(S812F) allele exerts adverse effects on the wt *Ret* allele and impairs development of the ENS and kidney, and the resulting phenotype recapitulates clinical manifestations of the HSCR patient harboring the *RET*(S811F) mutation.

To reveal molecular interactions between wt and mutant RET protein, we introduced plasmids expressing wt RET51 (long isoform of human RET), RET51(Y1062F), and RET51(S811F) into HEK293T cells. RET51(Y1062F) is a signaling-deficient RET mutant that has been shown to impair the physiological function of RET in vivo.[18] When wt RET51 alone was overexpressed, robust autophosphorylation of RET was detected (Figure 3*A*, lanes 1 and 7). In contrast, only marginal or no RET phosphorylation was detected when RET51(Y1062F) or RET51(S811F) was respectively overexpressed (Figure 3*A*, lanes 6 and 12). Co-expression of wt RET51 and RET51(Y1062F) with varying amounts of mutant plasmids did not show obvious changes in the phosphorylation levels of RET in any conditions (lanes 2–5). In contrast, co-expression of wt RET51 and RET51(S811F) resulted in a
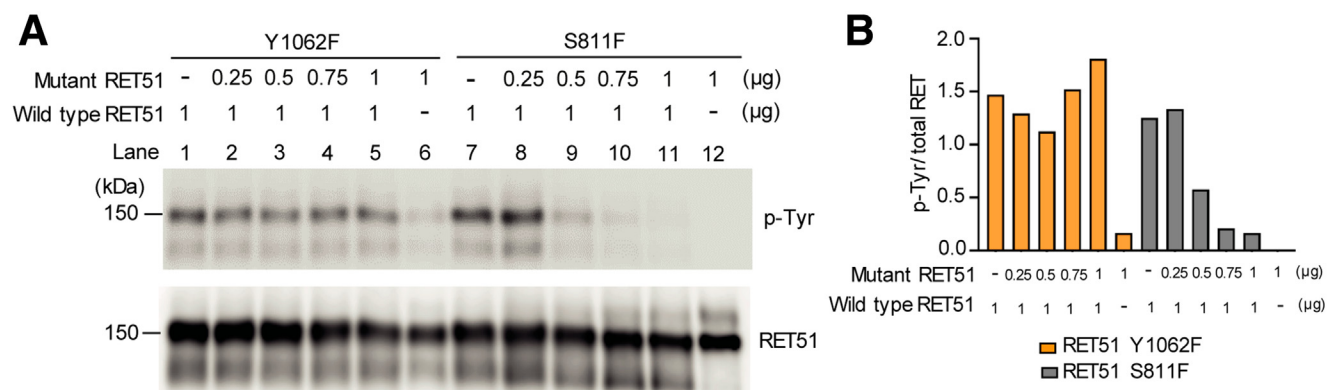

Figure 3. Ret(S812F) impairs ENS development via a dominant-negative mechanism. (*A*) Biochemical analysis of wt RET and RET(S811F) and their interactions. Panels show phosphorylated (*top*, immunoprecipitated RET51 blotted with anti-phospho-tyrosine antibodies) and total amounts of RET51 protein (*bottom*, reblotted with anti-RET51 antibodies). (*B*) Graph shows phosphorylation levels of RET obtained by normalization with total RET51 levels. Co-expression of wt RET51 and RET51(S811F) resulted in a dramatic decrease in RET phosphorylation.

dramatic decrease in RET phosphorylation, and this decrease occurred in a RET51(S811F) plasmid dose-dependent manner (Figure 3A, lanes 8–11, and B). The impaired phosphorylation of wt RET51 is presumably due to lack of transactivation in dimers formed between wt and the mutant RET. These biochemical data indicate that RET(S811F) is not only functionally impaired but also exerts dominant-negative actions on wt RET.

hKikumeGR
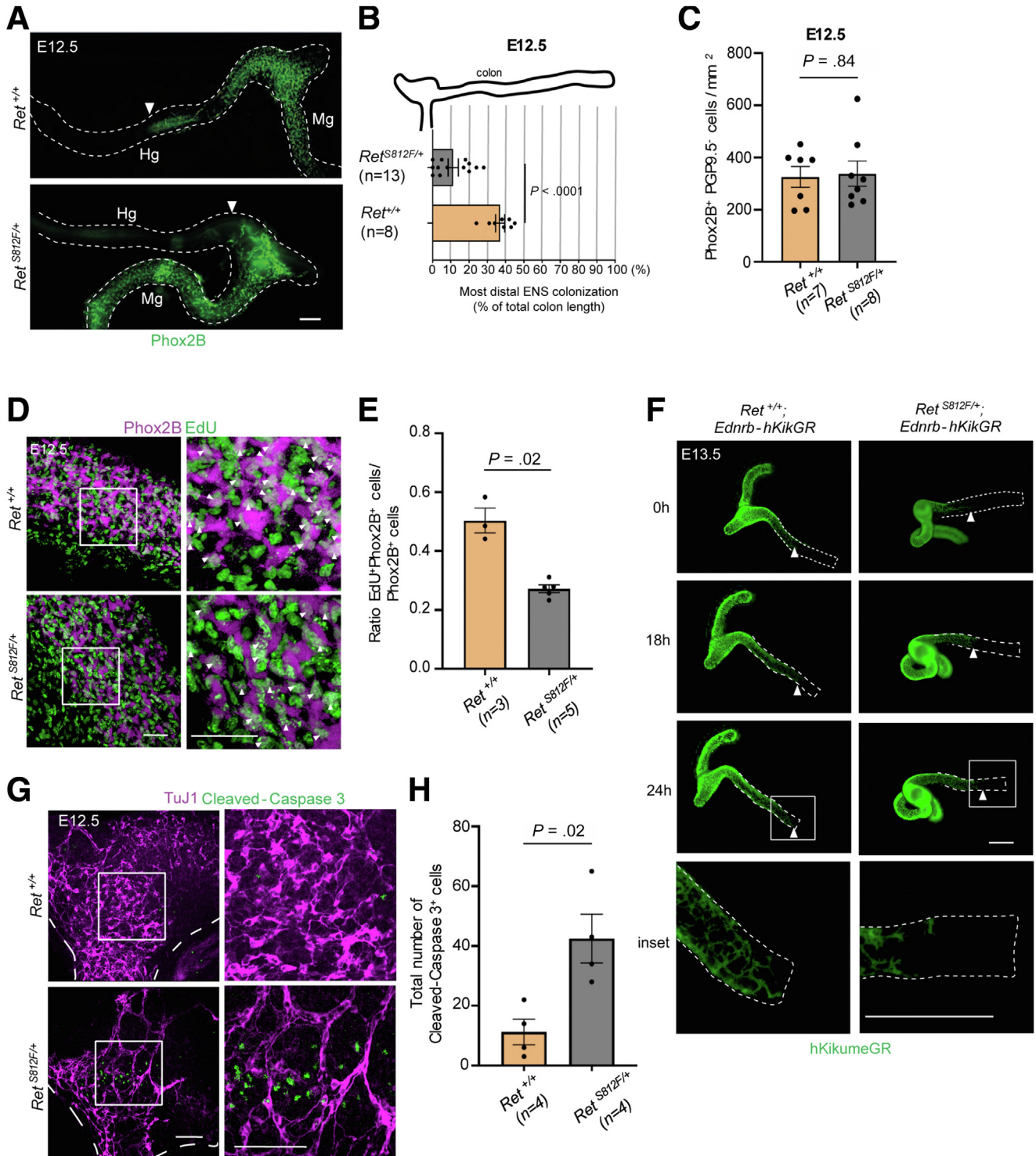
Ret(S812F) Impairs Migration, Proliferation, and Survival of ENS Progenitors

To understand how *Ret*(S812F) mutation affects development of the ENS, we examined $Ret^{S812F/+}$ embryos. We did not see obvious differences in the structure of the developing ENS by E11.5 (data not shown). However, gut colonization by ENS progenitors was delayed at E12.5 (Figure 4A and B). Phox2B and PGP9.5 double labeling revealed that progenitor density at the ileocecal junction was comparable (Figure 4C), but their proliferation was significantly impaired in $Ret^{S812F/+}$ embryos (Figure 4D and E). Time-lapse imaging of ENS progenitors using Ednrb-hKikGR[19] revealed that individual ENS progenitors showed impaired migration toward the distal portion of the hindgut (Figure 4F, Supplementary Videos 1 and 2). We also noted abnormal cell death at the proximal portion of the hindgut (Figure 4G and H, Figure 9). This cell death was not due to phototoxicity by time-lapse imaging because embryonic gut subjected to anti-cleaved caspase 3 staining immediately after dissection also revealed many stained cell bodies in the same area. Thus, ENS deficits in $Ret^{S812F/+}$ mice are caused by impaired migration, proliferation, and abnormal cell death of ENS progenitors that occur during mid-gestation (E12.5 and thereafter).

Adult $Ret^{S812F/+}$ Mice Exhibit Decreased Survival and Impaired Gut Function With Anatomic Abnormalities in the ENS

Most of $Ret^{S812F/+}$ mice grew into adulthood despite the presence of ENS deficits. Nonetheless, they did show decreased survival as compared with wt mice (approximately 20% of the mutant mice died by 30 weeks, Figure 5A). Body weight decrease was detected transiently in male mice at 2 months old, whereas it was more evident in female mutant mice at 1 and 3 months of age (Figure 5B). Total gastrointestinal transit time was significantly longer in 2-month-old $Ret^{S812F/+}$ mice than wt mice (Figure 5C). Moreover, water content in stool was reduced in $Ret^{S812F/+}$ mice as compared with wt mice (Figure 5D). Along with these changes, abnormal retention of stool was often detected in the distal colon of $Ret^{S812F/+}$ mice (Figure 5E). These observations revealed severe constipation in $Ret^{S812F/+}$ mice.

HSCR patients often display gut problems even after surgery, suggesting that there are deficits in the ENS of the ganglionated region. We examined neuron numbers and neuronal subtype specification in the ganglionated gut regions of adult $Ret^{S812F/+}$ mice. The numbers of myenteric and submucosal neurons detected by Phox2B and PGP9.5 immunohistochemistry, respectively, were significantly decreased in all gut regions of $Ret^{S812F/+}$ mice as compared with wt mice (Figure 6A, Figure 10). Nicotinamide adenine dinucleotide phosphate (NADPH)-diaphorase staining, which visualizes primarily inhibitory motor neurons and immuno-histochemistry of acetylcholinesterase expressing neurons, revealed that both neuron types were significantly reduced in number in the myenteric plexus of all gut regions (Figure 6B and C, Figure 11A and B). We also performed double staining using anti-Phox2B antibodies, which labels all enteric neurons, and antibodies detecting the neuronal subtype markers, calretinin, somatostatin, neuronal nitric oxide synthase (nNOS), or calbindin. The ratio of those individual neuronal subtypes in all enteric neurons was calculated. This analysis revealed gut region-dependent impairment in neuronal subtype specification. For instance, nNOS-positive neurons were decreased only in the distal colon. Calretinin-positive neurons were significantly decreased in the distal colon but not in the proximal colon and small intestine. Somatostatin-positive neurons did not show any significant differences in all gut regions, whereas calbindin-positive neurons were decreased in the proximal colon (Figure 6D–G, Figure 11C and D). $Ret^{S812F/+}$ mice thus display systemic neuron number decrease with selective and region-dependent impairment in neuronal subtype specification.

Ret(S812F) Displays Epistatic Interactions With Gene Mutations Conferring HSCR Susceptibility

Isolated HSCR is a multifactorial disorder and involves multiple gene mutations. It is therefore possible that HSCR patients with *RET* missense mutations carry other gene mutations as well. We examined whether the *Ret*(S812F) mutation interacts with other HSCR susceptibility genes and alters expressivity and severity of the ENS phenotype. The *RET9* allele is a *Ret* knock-in allele expressing RET9, a short isoform of RET, at lower levels than normal. $Ret^{RET9/-}$ mice

Figure 4. (*See previous page*). **Ret(S812F) impairs proliferation, migration, and survival of ENS progenitors.** (*A*) Whole-mount staining of embryonic gut (E12.5) using anti-Phox2B antibody. ENS progenitors of $Ret^{S812F/+}$ embryos displayed a delay in hindgut colonization at E12.5. *Arrowheads* depict the most caudally located ENS progenitors. (*B*) Graph shows ratio of most caudal Phox2B+ ENS cells to percent of total colon length at E12.5. Unpaired two-tailed *t* test with Welch's correction. (*C*) Graph shows ENS progenitor density (Phox2B+PGP9.5- cells) at the ileocecal junction was comparable between wt and $Ret^{S812F/+}$ at E12.5. Unpaired two-tailed *t* test with Welch's correction. (*D*) Representative images showing proliferating cell populations (labeled by EdU, *green*) in ENS progenitors (Phox2B+, *magenta*) at the ileocecal junction. (*E*) Graph shows ratio of EdU-incorporated ENS progenitors ($Ret^{+/+}$, n = 3; $Ret^{S812F/+}$, n = 5), unpaired two-tailed *t* test with Welch's correction. (*F*) Gut organ culture to assess migratory behaviors of ENS progenitors. *Bottom left panels* show complete colonization of the E13.5 gut by wt ENS progenitors observed after 24 hours. ENS progenitors of E13.5 $Ret^{S812F/+}$ embryos failed to reach the anal end (*bottom right panels*). Magnified pictures of insets (24 hours) shown in the bottom panels. (*G*) Immunohistochemical analysis of cell death (E12.5). Sparser distribution of enteric neurons (TuJ1+, *magenta*) in $Ret^{S812F/+}$ embryos than wt in the proximal hindgut (*left panels*), associated with noticeable increase in cleaved caspase 3-positive cells (*green*). Magnified pictures of insets shown in their *right panels*. (*H*) Graph shows quantification of numbers of cleaved caspase-3^{+} cells (n = 4 per group), unpaired two-tailed *t* test with Welch's correction. *Dashed lines* in (*A*), (*H*), and (*G*), gut margins; *arrowheads*, migratory wavefront of ENS progenitors. Hg, hindgut; Mg, midgut. Scale bars: (*A*) 50 μm, (*D* and *G*) 100 μm, (*F*) 500 μm.
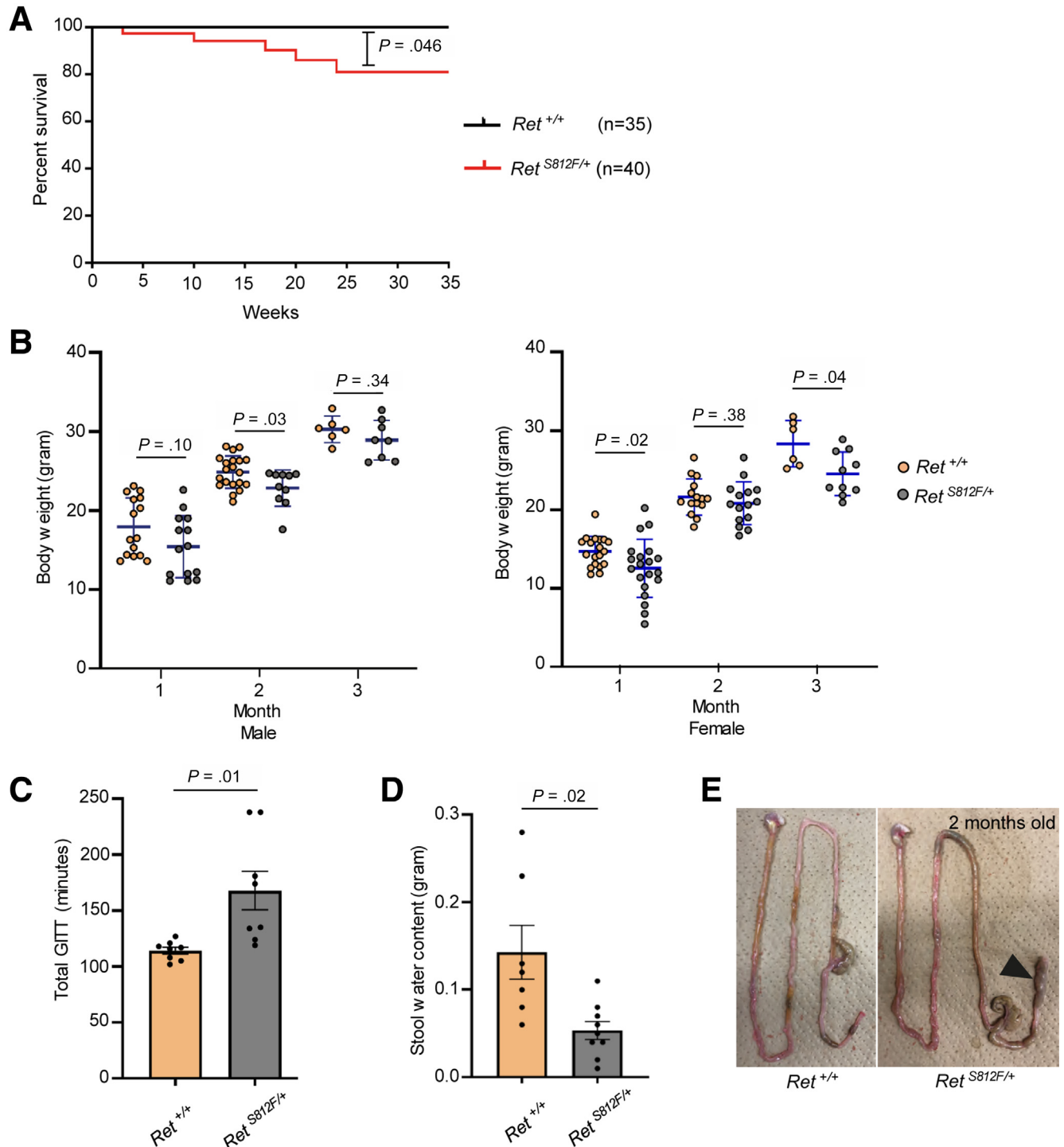
Figure 5. Adult $Ret^{S812F/+}$ mice exhibit decreased survival with impaired gut function. (*A*) Kaplan-Meier curves showing survival rate of $Ret^{+/+}$ (n = 35) and $Ret^{S812F/+}$ (n = 40) mice. Decreased survival rate observed in $Ret^{S812F/+}$ mice (log-rank test; *P* = .046). Kaplan–Meier survival function test. (*B*) Comparison of body weight of $Ret^{+/+}$ and $Ret^{S812F/+}$ mice from 1 to 3 months of age in each gender. Unpaired two-tailed *t* test with Welch's correction. (*C* and *D*) Functional analysis of the gut. Surviving 2-month-old $Ret^{S812F/+}$ mice displaying longer total gastrointestinal transit time (GITT) than wild-type control (*C*, n = 8 per group) and decreased water content in the stool (*D*, $Ret^{+/+}$, n = 7; $Ret^{S812F/+}$, n = 9), unpaired two-tailed *t* test with Welch's correction. (*E*) Abnormal retention of the stool (*arrowhead*) in the distal gut in $Ret^{S812F/+}$ mice.

display distal colon aganglionosis with incomplete penetrance.[20] The *RET9* allele therefore represents a hypomorphic *Ret* allele and partially mimics the *RET* enhancer mutation in that it confers susceptibility to HSCR. We crossed $Ret^{S812F/+}$ mice to $Ret^{RET9/+}$ mice and found that all $Ret^{S812F/RET9}$ mice display intestinal aganglionosis, indicating that these
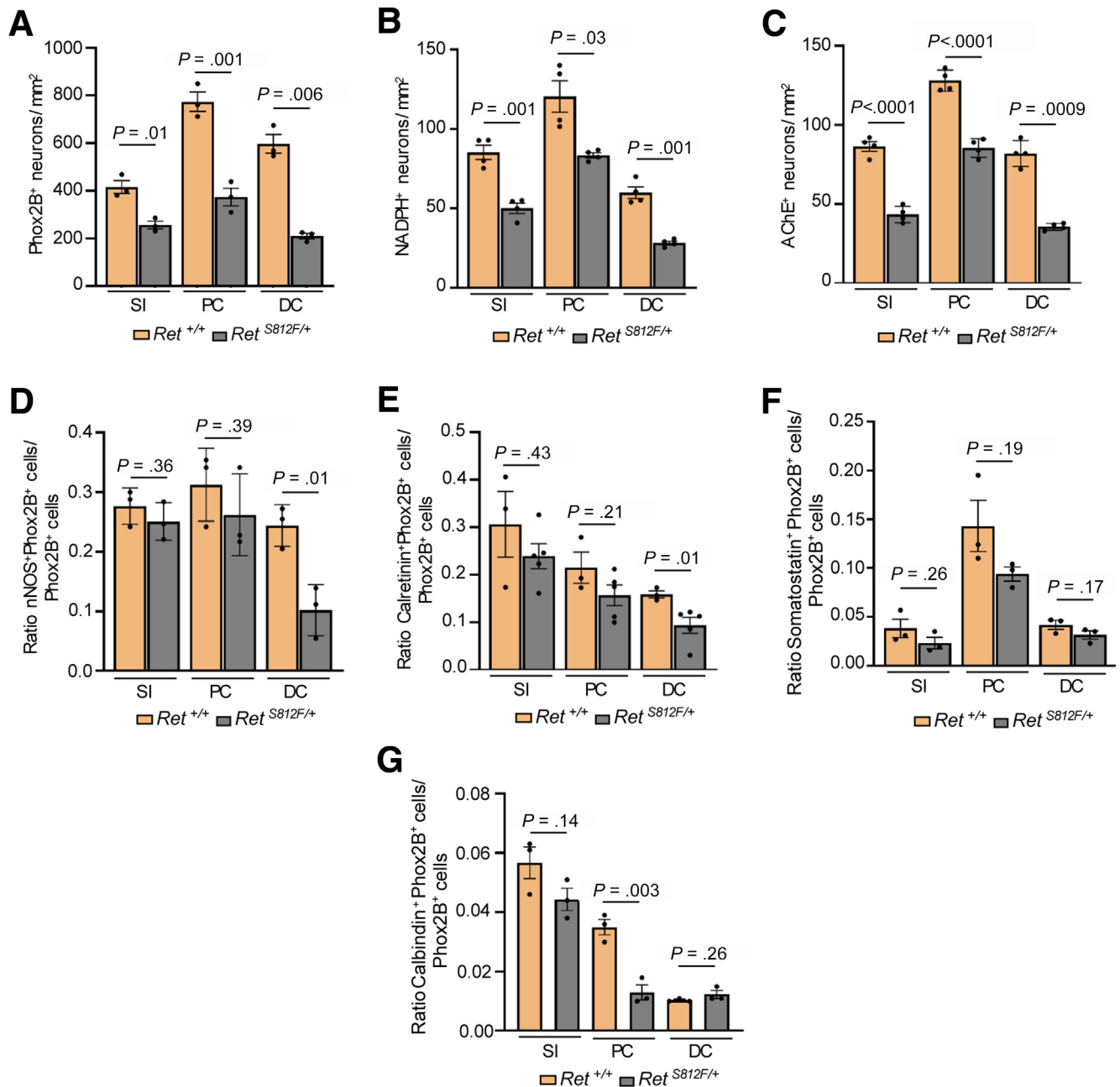
Figure 6. **Decreased numbers of enteric neurons and impaired neuronal subtype specification in ENS of *Ret*^*S812F/+*** **mice.** (*A*–*C*) Quantification of total numbers of Phox2B$^+$ (n = 3 per group) (*A*), NADPH-d$^+$ (n = 4 per group) (*B*), and acetylcholinesterase (AChE$^+$) neurons (n = 4 per group) (*C*). All gut regions showed significant decrease in enteric neuron numbers in *Ret*^*S812F/+*^ mice as compared with wt mice. (*D*–*G*) Ratio of enteric neuron subtypes (*D*, nNOS (n = 3 per group); *E*, calretinin (*Ret*^*+/+*^, n = 3; *Ret*^*S812F/+*^, n = 5); *F*, somatostatin (n = 3 per group); *G*, calbindin (n = 3 per group)). Unpaired two-tailed *t* test with Welch's correction. DC, distal colon; PC, proximal colon; SI, small intestine.

compound mutations exacerbate the phenotype (Table 1, Figure 7*A*, compare gray and orange bars). We further examined the interaction of the *Ret*(S812F) allele with the *Ednrb* gene. Previous studies showed that *RET* and the *Ednrb* genes are epistatic in HSCR patients and in mouse models of intestinal aganglionosis.[21] Crossings of *Ret*^*S812F/+*^ mice to

Ednrb^*+/-*^ mice revealed that all *Ret*^*S812F/+*^; *Ednrb*^*+/-*^ displayed intestinal aganglionosis at birth (Table 1, Figure 7*A* and *C*, bottom panels), which contrasted the normal ENS development seen in *Ret*^*+/-*^; *Ednrb*^*+/-*^ mice (Figure 7*C*, top panels). The aganglionic region was significantly longer in *Ret*^*S812F/+*^; *Ednrb*^*+/-*^ mice than *Ret*^*S812F/+*^ (only animals displaying
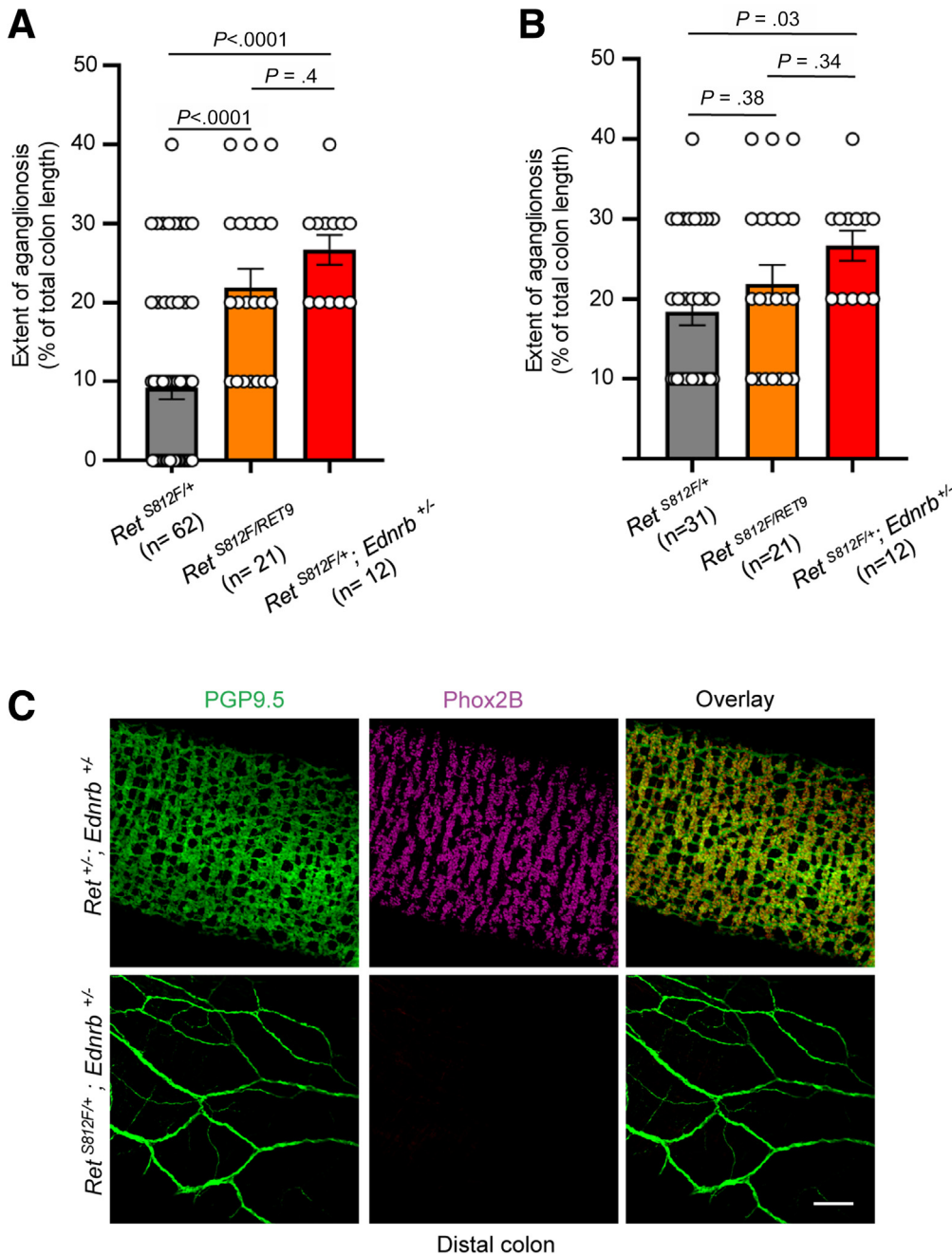
Figure 7. Epistatic interactions between the *Ret*(S812F) and HSCR susceptibility genes. (*A*) Severity of intestinal aganglionosis in $Ret^{S812F/+}$, $Ret^{S812F/RET9}$, and $Ret^{S812F/+}$; $Ednrb^{+/-}$ mice. (*B*) Comparison of length of aganglionic segment in $Ret^{S812F/+}$, $Ret^{S812F/RET9}$, and $Ret^{S812F/+}$; $Ednrb^{+/-}$ mice. One-way analysis of variance with Tukey multiple comparisons test. Note that *P* values differ on basis of the change in the numbers of $Ret^{S812F/+}$ mice. (*C*) Immunohistochemical analysis of newborn gut with PGP9.5 and Phox2b antibodies. Normal ENS development in $Ret^{+/-}$; $Ednrb^{+/-}$ (*top*) and intestinal aganglionosis in $Ret^{S812F/+}$; $Ednrb^{+/-}$ mice (*bottom*). Note absence of Phox2B immunoreactivity in $Ret^{S812F/+}$; $Ednrb^{+/-}$ mice. PGP9.5$^+$ nerve fibers in these mice likely represent extrinsic innervation. Scale bar: 100 μm.

intestinal aganglionosis were used for the comparison), but comparable with $Ret^{S812F/RET9}$ mice (Figure 7*B*). Approximately half of $Ret^{S812F/RET9}$ mice (8 of 17 mice) and $Ret^{S812F/+}$; $Ednrb^{+/-}$ mice (5 of 11 mice) died within 5 weeks after birth (Figure 12*A*). No difference was observed in the severity of intestinal aganglionosis between males and females of those compound mutant mice (Figure 12*C* and *D*). These results demonstrate strong epistasis between *Ret*(S812F) and the *Ednrb* gene in both expressivity and severity of the intestinal aganglionosis.

Discussion

In this study, we generated mice harboring a *Ret*(S812F) mutation, which was identified in a HSCR patient with unilateral kidney agenesis and oligomeganephronia. The $Ret^{S812F/+}$ mice recapitulated the patient's symptoms, and molecular analyses revealed that RET(S811F) is not only a null mutant but abrogates function of wt RET in a dominant-negative manner. This study demonstrates that a single *RET* missense mutation, which was identified in a HSCR patient, alone can induce intestinal aganglionosis in vivo. This

finding provides further insight into deeper understanding of the pathogenetic mechanism of HSCR by _RET_ mutations.

HSCR displays complex patterns of inheritance. In general, isolated HSCR displays a non-Mendelian mode of inheritance with low penetrance, sex bias, and variable length of aganglionic segments. In contrast, syndromic HSCR often shows Mendelian modes of inheritance. However, some non-syndromic HSCR families display autosomal dominant inheritance with incomplete penetrance.[12,22] In this study, we have found that all $Ret^{S812F/+}$ mice harbor deficits in the ENS, with either intestinal aganglionosis or hypoganglionosis (each with 50% incidence). About 10% of $Ret^{S812F/+}$ mice also had unilateral kidney agenesis, with the remaining kidney displaying reduced numbers of glomeruli. This relatively low penetrance of the kidney phenotype in $Ret^{S812F/+}$ mice is consistent with past observations that the development of the kidney is less sensitive to reduced RET function than that of the ENS. The incidence of the kidney phenotype in $Ret^{S812F/+}$ mice appears less common than in a series of 106 HSCR cases (20.7%).[23] With these genetic and phenotypic features, $Ret^{S812F/+}$ mice serve as a model for HSCR families with an isolated renal anomaly that display dominant inheritance with incomplete penetrance. This in turn suggests that in such HSCR families, some of the apparently unaffected siblings may actually have deficits in the ENS such as oligoganglionosis, as seen in half of $Ret^{S812F/+}$ mice. In this respect, it is interesting to note that a recent review pointed out a possible underdiagnosis of HSCR, especially in cases displaying oligoganglionosis-like histopathology.[1]

Genetic crossing of the _Ret_(S812F) allele with _RET9_ and _Ednrb_-deficient allele revealed their epistatic interactions on intestinal aganglionosis. All the $Ret^{S812F/RET9}$ mice and $Ret^{S812F/+}$; $Ednrb^{+/-}$ mice exhibited intestinal aganglionosis. When only mice with intestinal aganglionosis are considered, extent of aganglionosis segment is similar between $Ret^{S812F/+}$ and $Ret^{S812F/RET9}$ mice. In contrast, length of the aganglionic segment was significantly longer in $Ret^{S812F/+}$; $Ednrb^{+/-}$ mice than that of $Ret^{S812F/+}$. The kidney phenotype was exacerbated in $Ret^{S812F/RET9}$ mice (approximately 10% displaying bilateral renal agenesis, Table 1), whereas it appeared unchanged in $Ret^{S812F/+}$; $Ednrb^{+/-}$ mice. This difference reflects the physiological requirement of RET, but not EDNRB, signaling for kidney development. The stronger epistatic interaction with the _Ednrb_-deficient allele than with _RET9_ allele on the phenotype of the ENS, but not that of kidneys, suggests that the _Ednrb_ heterozygosity impairs signaling pathways other than those shared between RET and EDNRB signaling.[24] These results in epistatic interactions also suggest that inheritance patterns and severity of the aganglionic phenotype in HSCR are determined by the numbers and types of associated gene mutations. The stable shifts to the aganglionic phenotype by these genetic crossings demonstrate that the _RET_(S812F) allele represents one of the most sensitive _RET_ mutant alleles for assessing potential epistatic interactions between _RET_ mutations and other HSCR susceptibility genes.

Although gene targeting studies have revealed a number of genes whose disruption leads to intestinal aganglionosis

in mice,[20,25–29] establishing a HSCR mouse model has still not been a straightforward exercise. Even in mice harboring mutations in the _Ret_ gene, artificial genetic settings are required to develop the intestinal aganglionosis phenotype. To date, 9 types of Ret mutant alleles, including _Ret_-deficient,[3,30] _Ret51_,[31] _Ret_(C620R),[32] _Ret_(S697A),[33] _Ret_(Y981F),[34] _Ret_(Y1015F),[34] _Ret_(Y1062F),[18] _Ret_(RET9),[20] and _RetDN_ alleles,[35] have been reported to cause intestinal aganglionosis in mice. Among these, only C620R is a naturally occurring mutation identified in HSCR patients who also display MEN2A. However, $Ret^{C620R/+}$ mice do not show an overt intestinal aganglionosis phenotype, although the numbers of their enteric neurons appear to decrease. The other mutations were not identified in HSCR but were artificially generated for understanding the biological role of signaling pathways downstream of RET. In vivo, most of these mutant alleles require either homozygosity ($Ret^{-/-}$, $Ret^{51/51}$, $Ret^{C620R/C620R}$, $Ret^{S697A/S697A}$, $Ret^{Y981F/Y981F}$, $Ret^{Y1015F/Y1015F}$, $Ret^{Y1062F/Y1062F}$) or mono-allelic expression ($Ret^{RET9/-}$) to induce intestinal aganglionosis. Although the _RetDN_ allele alone ($Ret^{DN/+}$) can induce intestinal aganglionosis, the allele harbors double point mutations inadvertently generated during cloning in _RET9_ cDNA.[35] Collectively, to understand the pathologic significance of coding _RET_ mutations in HSCR, development of a novel HSCR mouse model carrying a natural HSCR mutation was required. The $Ret^{S812F/+}$ mice are the first HSCR mouse model that meets such a demand.

Because $Ret^{S812F/+}$ mice faithfully reproduce the genetic condition (heterozygous missense mutation) of the patient and recapitulate the clinical manifestations, these mice serve as a valuable platform to understand the pathology of HSCR. For instance, it is currently unknown why HSCR patients often continue to have gut problems even after surgery. In this respect, it is noteworthy that $Ret^{S812F/+}$ mice display a significant decrease in enteric neuron numbers throughout the gut and impaired differentiation in broad neuronal subtypes. This implies that differentiation of multiple neuronal subtypes depends on RET signaling, although it is currently unknown whether RET signaling functions in a permissive or instructive manner. Impaired neuronal differentiation may account, at least in part, for the persistent gut problems in HSCR patients. Physiological analysis of the gut in $Ret^{S812F/+}$ mice will elucidate how these anatomic changes influence the gut motility, neurotransmitter release, secretion, and blood flow. Such information will provide vital information toward development of novel strategies for postoperative management of HSCR.

$Ret^{S812F/+}$ mice can also be used as a model for developing new therapeutic strategies for HSCR. A single _Ret_(S812F) mutation induces ENS deficits (intestinal aganglionosis or hypoganglionosis) with 100% penetrance, which enables the efficient production of diseased mice. In addition, most of the $Ret^{S812F/+}$ mice (about 80%) survive up to 35 weeks. With their long survival and complete penetrant ENS deficits, $Ret^{S812F/+}$ mice serve as an ideal recipient for cell transplantation experiments. Moreover, scores of defecation problems are relatively constant among $Ret^{S812F/+}$ mice, which facilitates evaluation of the effects
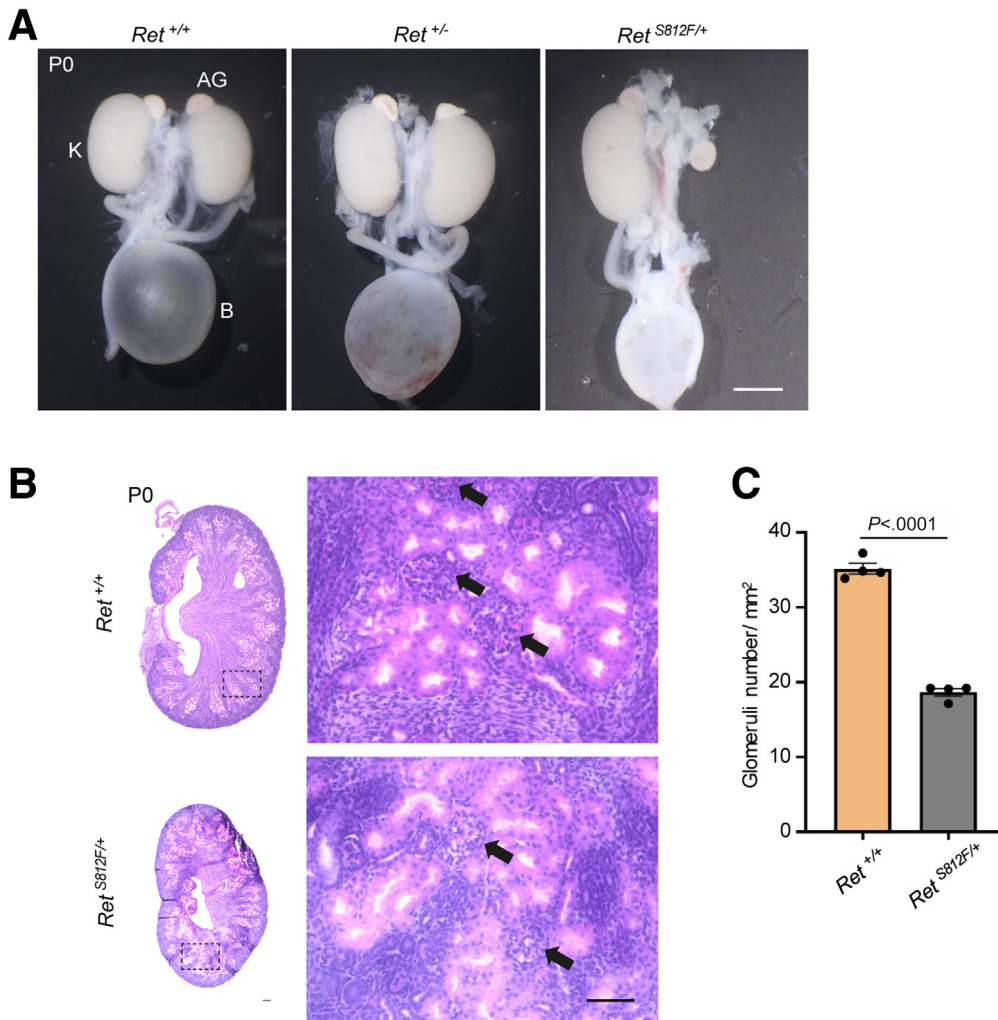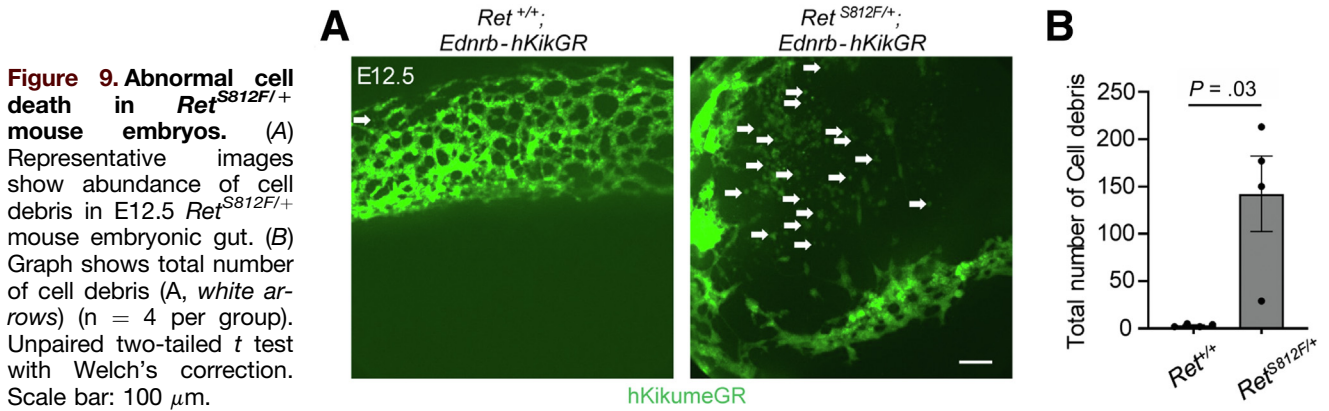
Figure 8. Renal abnormalities in $Ret^{S812F/+}$ mice. (*A*) Representative images showing unilateral kidney agenesis in $Ret^{S812F/+}$ mice. (*B*) Hematoxylin-eosin (HE) staining of kidney sections. Overall structure of remaining kidney in $Ret^{S812F/+}$ with unilateral kidney agenesis appeared grossly normal. (*C*) Graph shows density of glomeruli (B, *arrows* in right pictures) (n = 4 kidneys, 4 animals per group). Unpaired two-tailed *t* test with Welch's correction. AG, adrenal gland; B, bladder; K, kidney. Scale bar: (*A*) 0.1 cm, (*B*) 100 μm.

brought by cell transplantation. A recent study using some HSCR mouse models has shown that GDNF enema ameliorates intestinal aganglionosis by inducing enteric neurogenesis.[36] Because RET is a signaling receptor for GDNF, it will be interesting to examine whether GDNF exerts similar rescuing effects in $Ret^{S812F/+}$ mice. Such analyses will be required to assess the potential application of GDNF-induced enteric neurogenesis in HSCR patients in which *RET* mutations play a major role in their pathogenesis.

RET mutations in HSCR occur mostly in a heterozygous manner, and many of HSCR-associated *RET* mutations impair RET function in vitro. These observations have led to the notion that loss of function of RET on a single allele of the *RET* gene (RET heterozygosity) causes HSCR. However, some previous in vitro studies implied a potential dominant-negative action by HSCR-associated *RET* mutants.[37] Our study has clearly demonstrated the existence of such a dominant-negative mutant acting in vivo to induce intestinal aganglionosis. Our in silico analysis suggests that at least several HSCR-associated *RET* missense mutations in the kinase domain[8] exert the dominant-negative effect similar to that of RET(S811F) (Figure 13). Moreover, HSCR-associated coding *RET* mutations include many frameshift mutations that result in generation of a truncated RET protein.[4] Such RET mutants can act as dominant-negative mutants, which is similar to reports of other receptor tyrosine kinases.[38–40] Collectively, it is possible that a significant fraction of HSCR-associated *RET* mutants exhibit dominant-negative actions. In this respect, we may have to revise the current consensus that *RET* heterozygosity is sufficient to induce HSCR in humans. It is possible that similar to mice, induction of intestinal aganglionosis in humans requires impairment of RET function below half of its normal levels. To address this issue, it is necessary to investigate the exact amount of RET protein and levels of RET signaling in HSCR patients. Functional analysis of *RET* mutations in vivo is equally important. Recent advances in genome editing in mouse zygotes using electroporation enables production of mutant mouse strains in a short period of time at reasonable costs.[41] By generating a series of *RET* mutant mice with such a technology, an in vivo structure-function analysis will be possible. Such analyses will provide vital information toward better understanding of the pathogenesis of HSCR.

Figure 9. Abnormal cell death in *Ret*$^{S812F/+}$ mouse embryos. (*A*) Representative images show abundance of cell debris in E12.5 *Ret*$^{S812F/+}$ mouse embryonic gut. (*B*) Graph shows total number of cell debris (A, *white arrows*) (n = 4 per group). Unpaired two-tailed *t* test with Welch's correction. Scale bar: 100 μm.
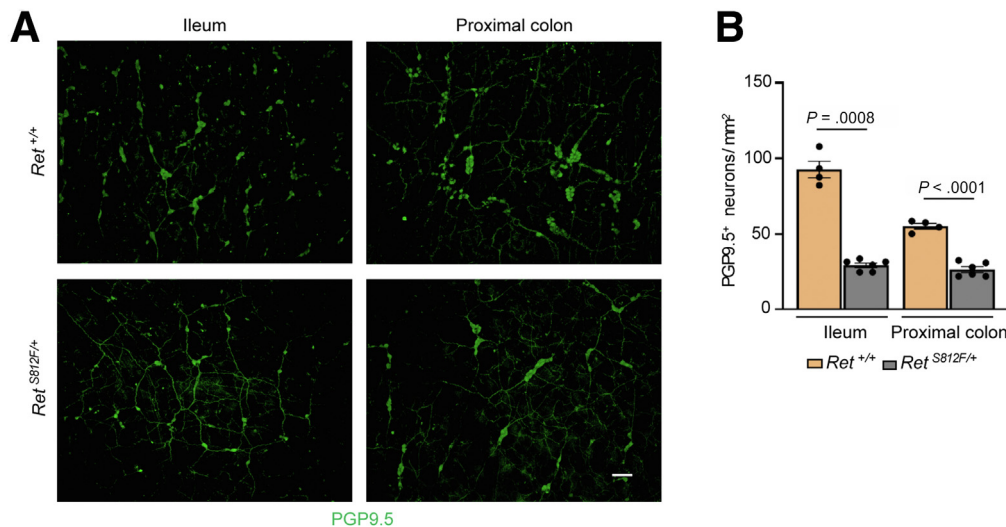
Methods

Animals

All procedures that include animal subjects were approved by the Institutional Animal Care and Use Committee (permission number: P200416) and carried out according to the Kobe University Animal Experimentation Regulations. The mouse lines used in this study were previously described: *Ret*$^{RET9/+}$,[20] *Ret*^{tlz},[15] and *Ednrb-hKikumeGR*,[19] *Ednrb*$^{+/-}$. Mice were bred and maintained at the Institute of Experimental Animal Research of Kobe University Graduate School of Medicine under specific pathogen-free conditions. The mice were housed in plastic cages (White PSF, CL-0123-3; CLEA Japan, Tokyo, Japan) with animal bedding (white flake, 9201100; Jackson Laboratory, Japan) at 25°C in a room with an automatically controlled 12-hour light: dark cycle. The mice were fed a normal diet (DC-8, 23.1% crude protein and 3590 kcal/kg; CLEA Japan) and had free access to water (mixture of hypochlorite water [50 ppm] and tap water [50 ppm], final concentration, 5–10 ppm).

Genotyping

Primer sequences for genotyping of mice were as follows: *Ret*$^{tauLacZ/+}$ using primers 5′-CAGCGCAGGTCTCTCATCAGTACCGCA-3′ (forward), 5′-ACGTCGCTTTCGCCATCGCCCGTGCGC-3′ (wild-type reverse), and 5′-AGGGCGAGGACAGTAGAGGGAGGCA-3′ (mutant reverse), *Ednrb-hKikume*, 5′-GAGATGAAGATCGAGCTGAGGATGG-3′ (forward) and 5′-TCTGCTTGAAGTAGTCCACGATCTC-3′ (reverse), *Ednrb*$^{+/-}$, 5′-CTGAGGAGAGCCTGATTGTGCCAC-3′ (forward) and 5′-CGACTCCAAGAAGCAACAGCTCG-3′ (reverse), *Ret*$^{RET9/+}$, 5′-CGAGACCCGCCTGCTCCTCAACCGC-3′ (forward), 5′-AGCGCTAACTTCACCCCGGCCCCTACCGTC-3′ (wild-type reverse), 5′-AGGCGGAAGCTGGGCACCTCCTCA-3′ (mutant reverse).

Generation of *Ret*$^{S812F/+}$ Mutant Mice

Female C57BL/6 mice at postnatal day 26–30 (P26–30) were superovulated by injection with 100 μL CARD HyperOva (Kyudo Company, Japan), followed by 7.5 IU intraperitoneal injection of human chorionic gonadotropin (Aska Pharmaceutical, Japan) 48 hours later. Sperm was
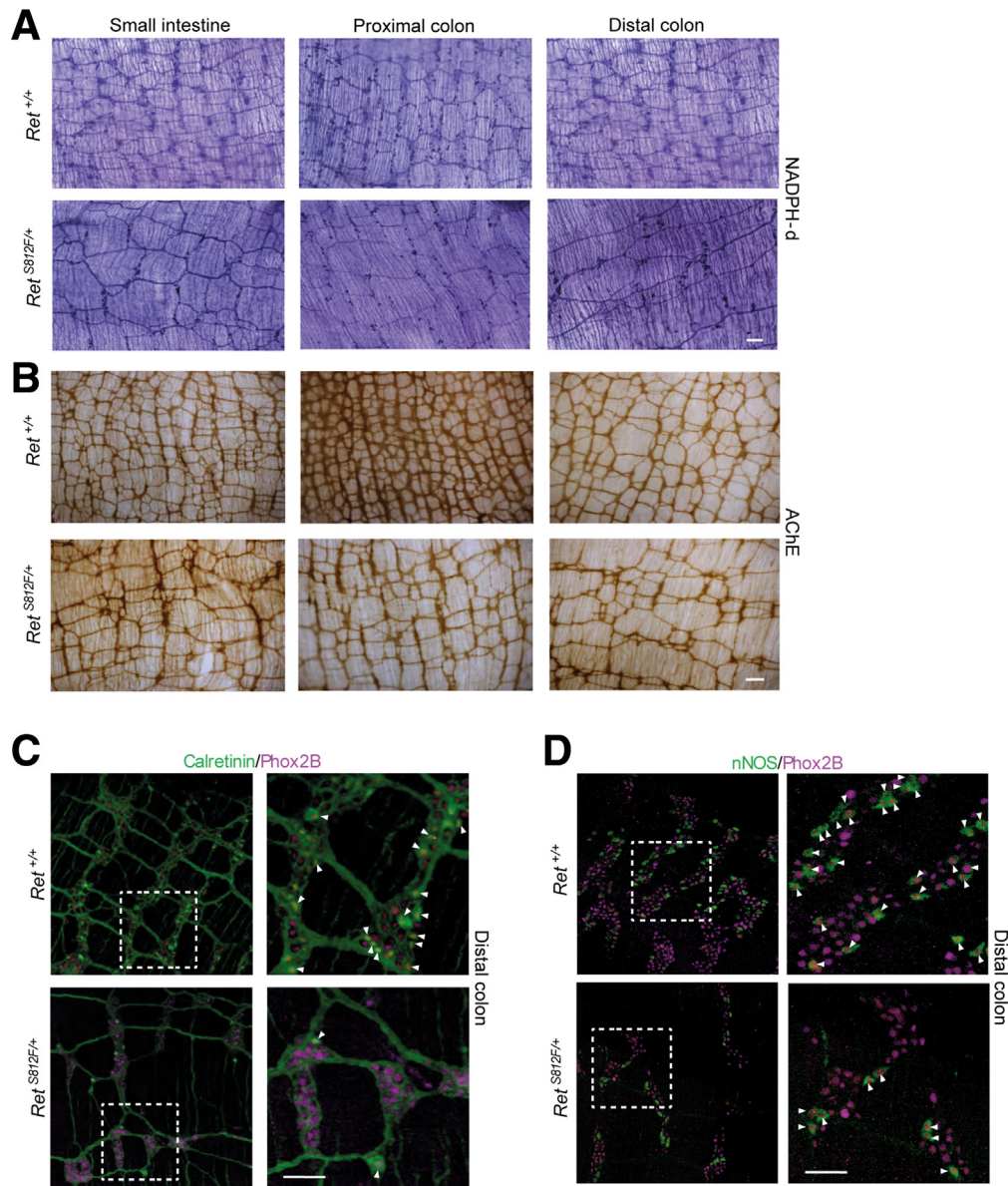

Figure 10. Enteric neuronal numbers in submucosal plexus are decreased in *Ret*$^{S812F/+}$ mice. (*A*) Whole-mount PGP9.5 staining of submucosal plexus in small intestine (*left*) and colon (*right*) of adult mice (2 months old). (*B*) Quantification of total number of PGP9.5$^+$ neurons in submucosal plexus (*Ret*$^{+/+}$, n = 4; *Ret*$^{S812F/+}$, n = 6). Unpaired two-tailed *t* test with Welch's correction. Scale bars: 100 μm.
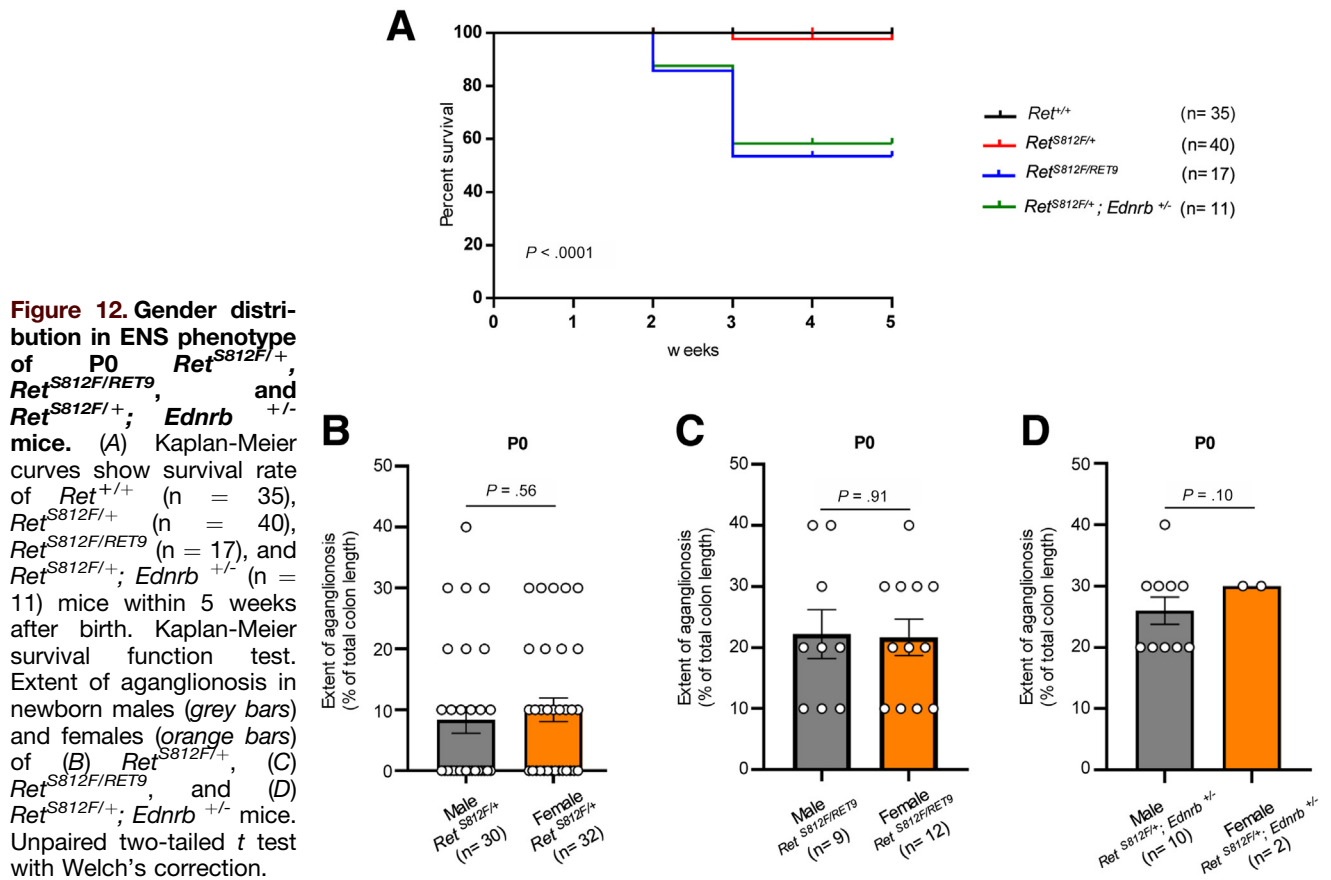
Figure 11. Histochemical analysis of enteric neurons and their differentiation. (*A*) Nicotinamide adenine dinucleotide phosphate-diaphorase (NADPH-d) staining. (*B*) Acetylcholinesterase (AChE) histochemistry. (*C* and *D*) Immunohistochemical detection of calretinin- (*C*) and nNOS- (*D*) expressing neuronal subtypes among enteric neurons (Phox2B$^+$). Scale bars: 100 μm.

collected from cauda epididymides of mature male C57BL/6 mice and incubated in human tubal fluid medium (101 mmol/L NaCl, 4.6 mmol/L KCl, 0.37 mmol/L KH$_2$PO$_4$, 0.2 mmol/L MgSO$_4$7H$_2$O, 25 mmol/L NaHCO$_3$, 2.78 mmol/L d-glucose, 2 mmol/L CaCl$_2$, 0.33 mmol/L Na-pyruvate, 21.4 mmol/L Na-lactate, 0.2 mmol/L penicillin G, 0.008 mmol/L streptomycin, 0.001 mmol/L phenol red, 0.004 mmol/L bovine serum albumin) for 1 hour at 37°C in a humidified incubator containing 5% CO$_2$. Ova were collected from the ampulla of the superovulated oviduct and mixed with 1.5 μL of sperm in human tubal fluid medium and incubated for 3 hours at 37°C. Fertilized eggs were collected in drops of modified Whitten's medium (109 mmol/L NaCl, 4 mmol/L KCl, 1 mmol/L KH$_2$PO$_4$, 2 mmol/L MgSO$_4$7H$_2$O, 22 mol/L NaHCO$_3$, 5 mmol/L d-glucose, 0.2 mmol/L Na-pyruvate, 2 mmol/L Ca-lactate, 0.2 mmol/L penicillin G, 0.008 mmol/L streptomycin, 0.001 mmol/

L phenol red, 0.01 mmol/L 2-mercaptoethanol, 0.05 mmol/L EDTA-2Na, 0.004 mmol/L bovine serum albumin), and washed 3 times by modified Whitten's medium to remove cumulus cells and extra sperms. Fertilized eggs were then washed with Opti-MEM I (Life Technologies, USA) to remove the serum-containing medium to facilitate the following electroporation.[41]

Electroporation

The 40–60 fertilized eggs were placed in a line within the electrode gap (LF501PT1-10, BEX, Japan) filled with total 5 μL volume of Opti-MEM I solution containing 0.24 μg/μL guide RNA (synthesized by Integrated DNA Technologies, USA), 0.5 μg/μL single-stranded oligo DNA nucleotides (synthesized by Eurofin Genomics, Luxembourg), and 0.2 μg/μL Cas9 protein (Integrated DNA Technologies). Electroporation was performed using CUY21

Figure 12. Gender distribution in ENS phenotype of P0 $Ret^{S812F/+}$, $Ret^{S812F/RET9}$, and $Ret^{S812F/+}$; $Ednrb^{+/-}$ mice. (*A*) Kaplan-Meier curves show survival rate of $Ret^{+/+}$ (n = 35), $Ret^{S812F/+}$ (n = 40), $Ret^{S812F/RET9}$ (n = 17), and $Ret^{S812F/+}$; $Ednrb^{+/-}$ (n = 11) mice within 5 weeks after birth. Kaplan-Meier survival function test. Extent of aganglionosis in newborn males (*grey bars*) and females (*orange bars*) of (*B*) $Ret^{S812F/+}$, (*C*) $Ret^{S812F/RET9}$, and (*D*) $Ret^{S812F/+}$; $Ednrb^{+/-}$ mice. Unpaired two-tailed *t* test with Welch's correction.

EDIT in vivo electroporator (BEX) with the subsequent conditions: 25 V (3 msec ON + 97 msec OFF) × 5 times. The sequences of the single-stranded oligo DNA nucleotides were as follows: *Ret (S812F): (*5′-TACCGAGACTGG-GCCCGACTCCTTGACTCTCTCTGTCCCCAGGGCCACTTCTTCT-CATTGTGGAGTATGCCAAGTATGGCTTCCTCCGGGGATTTCT-CCGTGACAGCCGCAAGATTGGGCCTGCCTATGTGAGCGGTGGA-GGCAGCCGCAACTCCAGCTC-3′). After electroporation, the eggs were collected immediately from the electrode gap and washed with modified Whitten's medium 3 times. The eggs were then cultured overnight in modified Whitten's medium at 37°C in a humidified incubator containing 5% CO_2. On the next day, surviving 2-cell stage zygotes were transferred into the oviducts of 0.5 days post-coitum pseudo-pregnant ICR females. The *Ret (S812F)* was genotyped as follows: PCR products amplified with primers (forward: 5′-GTGGTCAATGTAGGC-CAAGAGTGA-3′; reverse: 5′-GTCAGTACCCTTTCATCTGGGTGG-3′) were digested with MspI. The wt allele does not contain the Msp I site, resulting in 305 base pairs (bp), whereas the mutant allele results in 200 bp and 105 bp bands. PCR products of the mutant allele were cloned into a pBluescript vector and sequenced (Macrogen, Kyoto, Japan). *Ret (S812F)* missense mutation mice (mosaic F0) were identified by Sanger sequencing and then crossed with wt C57BL/6 mice to obtain F1 generation mice. All experiments were performed on mice with a C57BL/6 background.

Tissue Preparation and Histologic Analysis

For immunostaining, harvested small intestine (ileum) and colon tissue were placed in cold phosphate-buffered saline (PBS), open along the mesenteric border and pinned onto Silicone Elastomer (Sylgard 184; Dow Corning, Australia), serosa up, using insect pins. Muscle was peeled from the mucosa and submucosa to separate myenteric and submucosal plexus. Peeled gut was fixed overnight in 4% paraformaldehyde/PBS at 4°C. Samples were treated with 1% TritonX-100/PBS for 1 hour at room temperature to make them permeable as well as block non-specific staining. Samples were placed on a shaker, washed 3 times with PBS, each time for 30 minutes, and then primary antibodies were applied overnight at 4°C. After washing with PBS 3 times (30 minutes each), samples were incubated with secondary antibodies overnight at 4°C. Primary and secondary antibodies (Table 2) were applied in blocking solution. Immunofluorescence images were captured on a BZ-9000 microscope (Keyence, Japan) or a LSM 700 confocal microscope (Zeiss, Germany). For acetylcholinesterase staining, the tissue was postfixed in 4% paraformaldehyde/PBS for 1–2 hours at 4°C. The tissues were then transferred to saturated sodium sulfate and stored overnight at 4°C. The gut was then incubated in buffer (ethopropazine HCl [Sigma-Aldrich, USA] 0.2 mmol/L, acetylthiocholine iodide [Sigma-Aldrich] 4 mmol/L, glycine 10 mmol/L, cupric
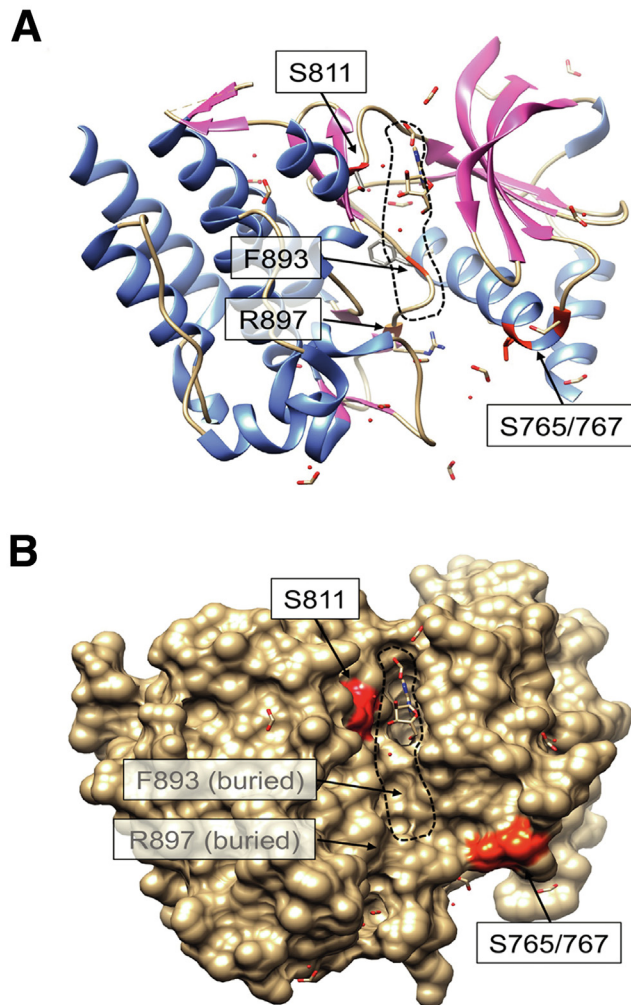
Figure 13. Spatial configuration of HSCR-associated missense mutations in the RET tyrosine kinase domain. (A) Ribbon model of the tyrosine kinase domain of human RET (Protein Data Bank ID: 4CKJ) constructed by UCSF Chimera software. *Dotted circle* shows an adenosine triphosphate (ATP)-binding pocket. Side chains of S765, S767, S811, F893, and R897 residues are shown. *Cyan and magenta ribbons* represent α-helices and β-strands, respectively. S811F mutation likely impairs binding of ATP to the kinase domain because of hindrance effect of bulky side chain of phenylalanine. F893L and R897Q mutations can partially disrupt the conformation of the ATP-binding pocket because both residues form the base under the bottom of the ATP-binding pocket. S765/767R mutations potentially change the opening width and electrostatic charge of the ATP-binding pocket, thereby preventing interaction of the kinase domain with ATP and/or substrates. (B) Space-filling model of (A). *Red and orange spheres* show molecular surfaces of S811 and S765/767 residues, respectively. Note that F893 and R897 residues are buried under the ATP-binding pocket.

sulfate 2 mmol/L, and sodium acetate 65 mmol/L, pH = 5.5) for 2–4 hours. Staining for acetylcholinesterase was developed by incubating for 1.5 minutes in sodium sulfide (1.25%, pH 6). Tissue was rinsed extensively with water before photographing under a dissecting microscope. High-power photomicrographs were obtained by opening the gut

along the mesenteric border, flattening the tissue with the serosal side up, and mounting in 50% glycerol before photographing.[42]

For NADPH-diaphorase staining,[43] tissue specimens that had been fixed in 4% paraformaldehyde/PBS for 1 hour at room temperature were rinsed with PBS and then were incubated in 1 mg/mL β-NADPH (Sigma-Aldrich), 0.1 mg/mL nitro blue tetrazolium (Sigma-Aldrich), and 0.3% Triton-X, 0.1 mol/L phosphate buffer (pH 7.4) at 37°C for 1 hour, until having a robust staining in the nitrergic neurons and nerves. After rinsing the specimens 3 times in distilled water for 10 minutes, they were mounted in 50% glycerol and were photographed.

For whole-mount 5-bromo-4-chloro-3-indolyl-β-D-galactoside (X-gal) staining,[44] embryos were fixed in 0.2% glutaraldehyde, 5 mmol/L EGTA, 2 mmol/L MgCl$_2$, 0.1% NP-40, 0.1 mol/L phosphate buffer (pH 7.2) for 30 minutes at 4°C and incubated in X-gal solution (0.01% sodium deoxycholate, 5 mmol/L potassium ferricyanide, 5 mmol/L potassium ferrocyanide, 0.1% NP-40, and 2 mmol/L MgCl$_2$ diluted in 0.1 mol/L phosphate buffer (pH 7.3), and add X-gal (5-bromo-4-chloro-3-indolyl-β-D-galactoside) (Nacalai Tesque, Japan) to a final concentration of 1 mg/mL before use for 4 hours at room temperature. Embryos were post-fixed in 4% paraformaldehyde to stop the reaction.

For 5-ethynyl-2′-deoxyuridine (EdU) staining, $Ret^{S812F/+}$ male crossed with wt C57BL/6 female mice. One milligram of EdU (Invitrogen, USA) was injected into pregnant mice at E12.5 intraperitoneally and killed 2 hours later. Peeled gut was fixed overnight in 4% paraformaldehyde/PBS at 4°C. Samples were treated with 0.3% TritonX-100/PBS for 20 minutes at room temperature, and then 5-ethynyl-2′-deoxyuridine Alexa Fluor 594 imaging kit (Invitrogen) solution was added. Samples were placed on a shaker for 30 minutes, washed with PBS, and mounted in 50% glycerol before photographing.

Images for bright-field were captured on EOS Kiss X5 camera (Canon, Japan), which were set under MZ FL III stereomicroscope (Leica, Germany). Representative images were selected from animals or experiments that had been repeated at least 3 times. Photoshop CC software (Adobe, USA) was used for global adjustments in levels, contrast, or brightness.

Cell Counts

The numbers of Phox2B-, nNOS-, calretinin-, somatostatin-, calbindin- acetylcholinesterase-, and NADPH-diaphorase-, PGP9.5-positive cells in myenteric or submucosal ganglia from the ileum, proximal-mid colon, and mid-distal colon were counted (manual counting) in 10 randomly selected fields of view (0.36 mm^2) (Phox2B, n = 5 per group; NADPH-diaphorase, n = 4 per group; acetylcholinesterase, $Ret^{+/+}$, n = 4; $Ret^{S812F/+}$, n = 3; nNOS, n = 3 per group; calretinin, $Ret^{+/+}$, n = 3; $Ret^{S812F/+}$, n = 5; somatostatin, n = 3 per group; calbindin, $Ret^{+/+}$, n = 3; $Ret^{S812F/+}$, n = 4; PGP9.5, $Ret^{+/+}$, n = 4; $Ret^{S812F/+}$, n = 7) captured with a 20× objective (Zeiss Axioskop 2 Plus). The

Table 2. List of Primary and Secondary Antibodies

Primary antibody	Dilution	Source	Catalog number	RRID
Mouse anti-Tuj1	1:1000	Covance	MMS-435P	AB_2313773
Rabbit anti-UCHL1/PGP9.5	1:500	Cosmo Bio	ABIN704396	AB_11184960
Guinea pig anti-Phox2B	1:700	Hideki Enomoto - Kobe University	Guinea pig anti-Phox2b (Enomoto 2012)	AB_2895590
Rabbit anti-Calretinin	1:500	Millipore	AB5054	AB_2068506
Rat anti-Somatostatin	1:200	Merck Millipore	MAB354	AB_2255365
Rabbit anti-Cleaved caspase-3	1:1000	Cell Signaling	9661	AB_2341188
Rabbit anti-Calbindin	1:1000	Millipore	AB1778	AB_2068336
Rat anti-nNOS	1:500	Invitrogen	61-7000	AB_88207
Goat anti-hRET (C-20)	1:1000	Santa Cruz Biotechnology Inc	sc-1290	AB_631316
Phospho-tyrosine (PY20)	1:2000	BD Biosciences	610007	AB_397428
Secondary antibody	Dilution	Source	Catalog number	RRID
CF488 donkey anti-rabbit IgG	1:500	Biotium	20015	AB_10559669
Alexa Fluor 488 goat anti-rat IgG	1:500	Thermo Fisher	A-1100	AB_2534074
CF488A donkey anti-mouse IgG	1:500	Biotium	20014	AB_10561327
CF568 goat anti-guinea pig IgG	1:500	Biotium	20108	AB_10559186
HRP-conjugated goat anti-rabbit	1:5000	Santa Cruz Biotechnology Inc	sc-2004	AB_631746
HRP-conjugated donkey anti-mouse	1:40,000	Jackson Immunoresearch	115-035-146	AB_2307392

proportions of $nNOS^+$, $calretinin^+$, and $somatostatin^+$ neurons to $Phox2B^+$ neuron ratio in myenteric ganglia were evaluated by normalizing the total number of $nNOS^+$, $calretinin^+$, and $somatostatin^+$ cells to $Phox2B^+$ neurons. For cell proliferation quantification, the proportion of EdU-positive cells was quantified in the ileocecal region from 3 wt and 5 $Ret^{S812F/+}$ E12.5 mouse embryos. For cell apoptosis quantification, the numbers of cleaved-caspase 3 positive cells were quantified in proximal hindgut of E12.5 mouse embryos from 4 mice per group.

Gut Organ Culture and Time-Lapse Imaging

Time-lapse imaging of enteric neural crest-derived cells (ENCCs) was performed using previously described methods.[19] Briefly, the embryonic whole guts (the midgut, cecum, and hindgut) from E12.5 $Ednrb\text{-}hKikumeGR; Ret^{S812F/+}$ mice were dissected with surrounding connective tissues and the mesentery. A half length of midgut was removed, and the midgut-mesentery junction was cut to make dissected guts straight. These midgut-cecum-hindgut samples were attached to a thin strip of filter membrane (Millipore) by pressing a part of connective tissues and the mesentery to the membrane strip. The gut-attached filter paper was suspended with the gut-side down on paraffin bridges streaked in parallel on a 35-mm glass-bottomed dish (IWAKI, Japan) to avoid direct contact of the gut tissue to the glass bottom. The guts were cultured in Dulbecco modified Eagle medium/F12 containing 10% fetal bovine serum and penicillin/streptomycin at 37°C with 5% CO_2 in a microscope incubation chamber and subjected to time-lapse imaging by an inverted fluorescent microscopy (Olympus IX81, Japan) equipped with confocal spinning disk unit (CSU-X1; Yokogawa Electric Corporation, Japan), high-

sensitive EMCCD camera (Hamamatsu Photonics, Japan), and Piezo motor (PI, Germany) for high-speed Z-scanning. The time-lapse system was controlled by Metamorph software (Molecular Device, USA). Z-series images (50–60 partially overlapping slices) were obtained every 5 minutes for 36 hours. Under these conditions, no obvious phototoxicity was observed.

To examine the migration assay, $Ednrb\text{-}hKikumeGR; Ret^{S812F/+}$ embryos at E13.5 were obtained by crossing $Ednrb\text{-}hKikume$ with $Ret^{S812F/+}$ mice. Cultured-gut samples were captured by immunofluorescence microscope at 0, 18, and 24 hours to evaluate the progression of ENS precursors in the colon of E13.5 mouse embryos.

Survival Analysis

Survival was determined by following the respective cohorts of animals weekly to determine mortality. Cohort sizes were as follows: wt, n = 35; $Ret^{S812F/+}$, n = 40 animals. Newborn mice (0-week) were defined as starting point, and 35-week-old mice were defined as endpoint. Mice that died, were dying, or did not move were considered to have died for these analyses. Dying mice were those that were unable or unwilling to walk and lack of response to manipulation. We analyzed survival by using the Kaplan–Meier survival function. Pairwise comparisons of survival curves were performed with a log-rank test.

Analysis of Body Weight, Gastrointestinal Motility, and Stool Water Content

Body weight of wt control and $Ret^{S812F/+}$ mice was assessed in the morning at 1 month, 2 months, and 3 months old by using a digital scale.

Gastrointestinal Motility Assays

Before the assay, mice had free access to food and water. Total gastrointestinal transit was assessed as previously described.[45] Briefly, mice were administered a solution of 6% carmine red dye (C1022-5G; Sigma-Aldrich) dissolved in 0.5% methylcellulose (M262-100G; Sigma-Aldrich) via oral gavage (10 μL per g of weight). For the total gastrointestinal transit, mice were then returned to individual cages without food, and cages were inspected every 5 minutes for the presence of red pellets. Total gastrointestinal transit was expressed as the time (in minutes) required from gavage to expulsion of the first red pellet.

Stool Collection

Stool collection and measurement were performed as described previously.[46] Each animal was removed from its home cage and placed in a clean, clear plastic cage without food or water for 1 hour. Stools were collected immediately after expulsion and sealed in preweighted tubes. The total stools were weighed to provide a wet weight, dried at $65°C$ overnight, and weighed again to provide a dry weight. The difference between wet and dry weights of stool was measured as the stool water content.

Generation of hRET51 (S811F)-Expression Plasmid

Insertion of S811F mutation into human RET51 cDNA was done according to the standard PCR-based site-directed mutagenesis protocol (Toyobo). Primers (forward: 5'-TGGAGTACGCCAAATACGGCTTCCTGCGGGGCTTCCTCCG-3'; reverse: 5'-TCGCGGAGGAAGCCCCGCAGGAAGCCGTATTT-GGCGTACT-3') containing the S811F mutation were used. The PCR products were then treated with DpnI to destroy the parental methylated DNA from the newly synthesized unmethylated mutant DNA and transformed into *Escherichia coli*. The mutagenized plasmid was taken up and then replaced the wt fragment with mutated fragment DNA into human Ret51 cDNA inserted into the pcDNA3.1 (Thermo Fisher Scientific, USA). The inserted mutant Ret51 cDNA was sequenced to confirm that proper mutation was introduced.

Immunoprecipitation

HEK293T cells that were cultured in 5% CO_2 in Dulbecco modified Eagle medium supplemented with 10% fetal bovine serum without coating were plated on a 6-well culture dish at $2.5–4 \times 10^5$ cells/well 1 day before transfection. The cells were transfected with expression vectors encoding RET51 and its point mutants by using FuGENE6 transfection reagent (Promega) according to the manufacturer's instructions. The transfected cells were washed twice with ice-cold PBS at 24–36 hours after transfection and then lysed with lysis buffer (Tris-buffered saline [pH 7.4] containing 1 mmol/L EGTA, 1 mmol/L EDTA, 1% Triton X-100, 0.5% NP-40, 5 mmol/L sodium pyrophosphate, 10 mmol/L NaF, 1 mmol/L Na3VO4, 10 mmol/L β-glycerophosphate, and 1 mmol/L phenylmethylsulfonyl fluoride). After centrifugation at 15,000 rpm for 20 minutes at $4°C$, the supernatants were incubated with 1 μg of goat anti-Ret51 antibody (C-20; Santa Cruz Biotechnology) and 30 μL of Protein G-Sepharose beads (50% slurry; GE Healthcare) overnight at $4°C$ with gentle agitation. Fifty microliters of $1\times$ sodium dodecyl sulfate-polyacrylamide gel electrophoresis sample buffer (50 mmol/L Tris-HCl [pH 6.8], 2% sodium dodecyl sulfate, 10% glycerol, and 5% beta-mercaptoethanol) was added to the beads after 3 times washing with ice-cold lysis buffer and then boiled for 5 minutes. Five microliters of samples was subjected to sodium dodecyl sulfate-polyacrylamide gel electrophoresis.

Immunoblotting

After transfer to the nitrocellulose membranes (GE; 10600004), they were blocked with Tris-buffered saline containing 3% skim milk and 0.05% Tween-20 and probed with primary antibody diluted in blocking buffer overnight at $4°C$. Primary antibodies were as follows: phospho-tyrosine (PY20, BD transduction; 610007, 1:2000), RET51 (Santa Cruz Biotechnology; C-20, AB_631316, 1:1000). After washing with Tris-buffered saline containing 0.05% Tween-20 three times, the membrane was probed with corresponding secondary antibody (horseradish peroxidase–conjugated goat anti-rabbit, Santa Cruz Biotechnology, sc-2004, 1:5000; horseradish peroxidase–conjugated donkey anti-mouse, Jackson Immunoresearch, AB_2307392, 1:40,000). Bound antibody was visualized with Supersignal West Dura kit (Thermo Fisher) and imaged with AI600 imager (GE Healthcare).

Glomerular Counting

Glomerular number was analyzed in $Ret^{+/+}$ mouse kidneys and smaller size of $Ret^{S812F/+}$ mouse kidneys at postnatal day 0 (P0). Kidneys were fixed for 24 hours in Bouin's solution (Sigma-Aldrich), embedded in paraffin, sectioned at 7 μm, and stained with hematoxylin-eosin. Glomerular numbers were estimated by counting the number of glomeruli in 20 randomly selected field-of-view (n = 4 kidneys, 4 animals per group), captured on a BZ-9000 Keyence microscope (bright-field image). The number of glomeruli per field-of-view was then converted to per mm^2.

Statistics

We used GraphPad Prism 5 (GraphPad Software) software. The experimental data are shown as means $\pm$ standard error of the mean. The unpaired two-tailed t test with Welch's correction was used for all experiments except Figure 7 (one-way analysis of variance with Tukey multiple comparisons test). Survival data were plotted by the Kaplan–Meier method and analyzed by the log-rank test. A cutoff of $P < .05$ was considered as statistically significant, and in each figure, P value was provided.

All authors had access to the study data and reviewed and approved the final manuscript.

References

1. Kapur RP, Ambartsumyan L, Smith C. Are we under-diagnosing Hirschsprung disease? Pediatr Devel Pathol 2020;23:60–71.

2. Airaksinen MS, Saarma M. The GDNF family: signalling, biological functions and therapeutic value. Nat Rev Neurosci 2002;3:383–394.

3. Schuchardt A, D'Agati V, Larsson-Blomberg L, et al. Defects in the kidney and enteric nervous system of mice lacking the tyrosine kinase receptor Ret. Nature 1994; 367:380–383.

4. Amiel J, Sproat-Emison E, Garcia-Barcelo M, et al. Hirschsprung disease, associated syndromes and genetics: a review. J Med Genet 2008;45:1–14.

5. Romeo G, Ronchetto P, Luo Y, et al. Point mutations affecting the tyrosine kinase domain of the RET proto-oncogene in Hirschsprung's disease. Nature 1994; 367:377–378.

6. Edery P, Lyonnet S, Mulligan LM, et al. Mutations of the RET proto-oncogene in Hirschsprung's disease. Nature 1994;367:378–380.

7. Pasini B, Borrello MG, Greco A, et al. Loss of function effect of RET mutations causing Hirschsprung disease. Nat Genet 1995;10:35–40.

8. Iwashita T, Kurokawa K, Qiao S, et al. Functional analysis of RET with Hirschsprung mutations affecting its kinase domain. Gastroenterology 2001;121:24–33.

9. Amiel J, Lyonnet S. Hirschsprung disease, associated syndromes, and genetics: a review. J Med Genet 2001; 38:729–739.

10. Heanue TA, Pachnis V. Enteric nervous system development and Hirschsprung's disease: advances in genetic and stem cell studies. Nat Rev Neurosci 2007; 8:466–479.

11. Nakatani T, Iwasaki M, Yamamichi A, et al. Point mutagenesis in mouse reveals contrasting pathogenetic effects between MEN2B- and Hirschsprung disease-associated missense mutations of the RET gene. Development, Growth & Differentiation 2020; 62:214–222.

12. Bolk S, Pelet A, Hofstra RM, et al. A human model for multigenic inheritance: phenotypic expression in Hirschsprung disease requires both the RET gene and a new 9q31 locus. Proc Natl Acad Sci U S A 2000; 97:268–273.

13. Seri M, Yin L, Barone V, et al. Frequency of RET mutations in long- and short-segment Hirschsprung disease. Hum Mutat 1997;9:243–249.

14. Sugimoto K, Miyazawa T, Nishi H, et al. Heterozygous p.S811F RET gene mutation associated with renal agenesis, oligomeganephronia and total colonic aganglionosis: a case report. BMC Nephrol 2016; 17:146.

15. Gould TW, Yonemura S, Oppenheim RW, et al. The neurotrophic effects of glial cell line-derived neurotrophic factor on spinal motoneurons are restricted to fusimotor subtypes. J Neurosci 2008;28:2131–2146.

16. Sunardi M, Ito K, Enomoto H. Live visualization of a functional RET-EGFP chimeric receptor in homozygous knock-in mice. Development, Growth & Differentiation 2021;63:285–294.

17. Heanue TA, Pachnis V. Ret isoform function and marker gene expression in the enteric nervous system is conserved across diverse vertebrate species. Mech Dev 2008;125:687–699.

18. Jijiwa M, Fukuda T, Kawai K, et al. A targeting mutation of tyrosine 1062 in Ret causes a marked decrease of enteric neurons and renal hypoplasia. Mol Cell Biol 2004; 24:8026–8036.

19. Nishiyama C, Uesaka T, Manabe T, et al. Trans-mesenteric neural crest cells are the principal source of the colonic enteric nervous system. Nat Neurosci 2012; 15:1211–1218.

20. Uesaka T, Nagashimada M, Yonemura S, et al. Diminished Ret expression compromises neuronal survival in the colon and causes intestinal aganglionosis in mice. J Clin Invest 2008;118:1890–1898.

21. Carrasquillo MM, McCallion AS, Puffenberger EG, et al. Genome-wide association study and mouse model identify interaction between RET and EDNRB pathways in Hirschsprung disease. Nat Genet 2002;32:237–244.

22. Badner JA, Sieber WK, Garver KL, et al. A genetic study of Hirschsprung disease. Am J Hum Genet 1990; 46:568–580.

23. Pini Prato A, Rossi V, Mosconi M, et al. A prospective observational study of associated anomalies in Hirschsprung's disease. Orphanet J Rare Dis 2013;8:184.

24. Chatterjee S, Chakravarti A. A gene regulatory network explains RET-EDNRB epistasis in Hirschsprung disease. Hum Mol Genet 2019;28:3137–3147.

25. Kapur RP. Early death of neural crest cells is responsible for total enteric aganglionosis in Sox10(Dom)/Sox10(Dom) mouse embryos. Pediatr Dev Pathol 1999; 2:559–569.

26. Shen L, Pichel JG, Mayeli T, et al. Gdnf haploinsufficiency causes Hirschsprung-like intestinal obstruction and early-onset lethality in mice. Am J Hum Genet 2002;70:435–447.

27. Bergeron KF, Cardinal T, Toure AM, et al. Male-biased aganglionic megacolon in the TashT mouse line due to perturbation of silencer elements in a large gene desert of chromosome 10. PLoS Genetics 2015;11:e1005093.

28. Li HB, Jin XQ, Jin X, et al. BMP4 knockdown of NCSCs leads to aganglionosis in the middle embryonic stage. Mol Med Rep 2018;17:5423–5427.

29. Okamoto M, Uesaka T, Ito K, et al. Increased RET activity coupled with a reduction in the RET gene dosage causes intestinal aganglionosis in mice. eNeuro 2021;8.

30. Enomoto H, Crawford PA, Gorodinsky A, et al. RET signaling is essential for migration, axonal growth and axon guidance of developing sympathetic neurons. Development 2001;128:3963–3974.

31. de Graaff E, Srinivas S, Kilkenny C, et al. Differential activities of the RET tyrosine kinase receptor isoforms during mammalian embryogenesis. Genes Dev 2001; 15:2433–2444.

32. Carniti C, Belluco S, Riccardi E, et al. The Ret(C620R) mutation affects renal and enteric development in a mouse model of Hirschsprung's disease. Am J Pathol 2006;168:1262–1275.

33. Asai N, Fukuda T, Wu Z, et al. Targeted mutation of serine 697 in the Ret tyrosine kinase causes migration

defect of enteric neural crest cells. Development 2006; 133:4507–4516.

34. Jain S, Knoten A, Hoshi M, et al. Organotypic specificity of key RET adaptor-docking sites in the pathogenesis of neurocristopathies and renal malformations in mice. J Clin Invest 2010;120:778–790.

35. Jain S, Naughton CK, Yang M, et al. Mice expressing a dominant-negative Ret mutation phenocopy human Hirschsprung disease and delineate a direct role of Ret in spermatogenesis. Development 2004;131: 5503–5513.

36. Soret R, Schneider S, Bernas G, et al. Glial cell-derived neurotrophic factor induces enteric neurogenesis and improves colon structure and function in mouse models of Hirschsprung disease. Gastroenterology 2020; 159:1824–1838 e17.

37. Cosma MP, Cardone M, Carlomagno F, et al. Mutations in the extracellular domain cause RET loss of function by a dominant negative mechanism. Mol Cell Biol 1998; 18:3321–3329.

38. Amaya E, Musci TJ, Kirschner MW. Expression of a dominant negative mutant of the FGF receptor disrupts mesoderm formation in Xenopus embryos. Cell 1991; 66:257–270.

39. Dumont DJ, Gradwohl G, Fong GH, et al. Dominant-negative and targeted null mutations in the endothelial receptor tyrosine kinase, tek, reveal a critical role in vasculogenesis of the embryo. Genes Dev 1994; 8:1897–1909.

40. Vajkoczy P, Knyazev P, Kunkel A, et al. Dominant-negative inhibition of the Axl receptor tyrosine kinase suppresses brain tumor cell growth and invasion and prolongs survival. Proc Natl Acad Sci U S A 2006; 103:5799–5804.

41. Hashimoto M, Takemoto T. Electroporation enables the efficient mRNA delivery into the mouse zygotes and facilitates CRISPR/Cas9-based genome editing. Sci Rep 2015;5:11315.

42. Enomoto H, Araki T, Jackman A, et al. GFR alpha1-deficient mice have deficits in the enteric nervous system and kidneys. Neuron 1998;21:317–324.

43. Enomoto H, Araki T, Jackman A, et al. GFR a1-deficient mice have deficits in the enteric nervous system and kidneys. Neuron 1998;21:317–324.

44. Enomoto H, Hughes I, Golden J, et al. GFRalpha1 expression in cells lacking RET is dispensable for organogenesis and nerve regeneration. Neuron 2004; 44:623–636.

45. Kimball ES, Palmer JM, D'Andrea MR, et al. Acute colitis induction by oil of mustard results in later development of an IBS-like accelerated upper GI transit in mice. Am J Physiol Gastrointest Liver Physiol 2005;288:G1266–G1273.

46. Greene JG, Noorian AR, Srinivasan S. Delayed gastric emptying and enteric nervous system dysfunction in the rotenone model of Parkinson's disease. Exp Neurol 2009;218:154–161.